UPPSALA
UNIVERSITET

Digital Comprehensive Summaries of Uppsala Dissertations from the Faculty of Science and Technology 686

Magnetic and Structural Properties of *f*-electron Systems from First Principles Theory

TORBJÖRN BJÖRKMAN

ACTA
UNIVERSITATIS
UPSALIENSIS
UPPSALA
2009

ISSN 1651-6214
ISBN 978-91-554-7644-1
urn:nbn:se:uu:diva-109639

Dissertation presented at Uppsala University to be publicly examined in A80101, Lägerhyddsvägen 1, Uppsala, Friday, December 4, 2009 at 13:15 for the degree of Doctor of Philosophy. The examination will be conducted in English.

Abstract
Björkman, T. 2009. Magnetic and Structural Properties of *f*-electron Systems from First Principles Theory. Acta Universitatis Upsaliensis. *Digital Comprehensive Summaries of Uppsala Dissertations from the Faculty of Science and Technology* 686. 82 pp. Uppsala. ISBN 978-91-554-7644-1.

A series of studies of *f*-electron systems based on density functional theory methods have been performed. The focus of the studies has been on magnetic and structural properties, as well as investigating ways to handle strong electron correlation in these systems.

A version of the self-interaction correction (SIC) method has been developed for a full-potential linear muffin-tin orbital method. The method is demonstrated to have the strong capabilities of previous SIC implementations, to study energetics and phase stabilities of *d*- and *f*-electron systems with localisation-delocalisation transitions, but with no geometrical constraints from the underlying band structure method. The method is applied to the high-T_C superconductor CeOFeAs, in which the *f*-shell of the Ce atoms is argued to undergo a Mott transition to a delocalised state under pressure.

The non-collinear magnetic structures of two rare earth compounds, $TbNi_5$ and $CeRhIn_5$ have been studied, and in both cases the complex magnetic ordering can be attributed to the effects of Fermi surface nesting.

The magnetic properties of the $FeMnP_{0.75}Si_{0.25}$ system has been studied and found to have an extreme sensitivity to the amount of disorder of the Fe-Mn sublattice.

Elements with valence *f* electrons typically exhibit very complex phase diagrams, with the frequently occurring phenomenon that they melt from a bcc phase that is unstable in calculations based solely on the electronic structure. The high temperature bcc phase of the elements La and Th were studied by means of the self-consistent ab initio lattice dynamics method that accounts for phonon-phonon interaction.

Delicate magnetic and structural properties are often sensible to details of how the Brillouin zone (BZ) integration is performed. An improved scheme is proposed that adapts to the BZ mesh and allows for better energy convergence of small energy differences in the smearing type methods.

Correlation effects in the 5*f*-states of plutonium has in recent years been the focus of attention for many theoretical studies employing extensions to DFT schemes. These different schemes have often produced large variations in 5*f* occupation numbers, and therefore a survey was made of experimental occupation numbers and 4*f* core level shifts to establish a value for the 5*f* occupation without any computational bias.

Torbjörn Björkman, Department of Physics and Materials Science, Materials Theory, Box 530, Uppsala University, SE-75121 Uppsala, Sweden

ISSN 1651-6214
ISBN 978-91-554-7644-1
urn:nbn:se:uu:diva-109639 (http://urn.kb.se/resolve?urn=urn:nbn:se:uu:diva-109639)

Till Heidi och Hillevi

List of Papers

This thesis is based on the following papers, which are referred to in the text by their Roman numerals.

I Björkman, T., Wills, J. M., Andersson, P. H. and Eriksson, O. Self-interaction correction scheme for a full-potential linear muffin-tin orbital method . (2009) *Submitted to Physical Review B*

II Björkman, T. and Eriksson, O. Theoretical investigation of the volume collapse of CeOFeAs under pressure. (2009) *In manuscript*

III Lizárraga, R., Bergman, A., Björkman, T., Liu, H.-P., Andersson, Y., Gustafsson, T., Kuchin, A. G., Ermolenko, A. S., Nordström, L. and Eriksson, O. (2006) Crystal and magnetic structure investigation of $TbNi_{5-x}Cu_x$ (x=0, 0.5, 1.0, 1.5, 2.0): Experiment and theory. *Physical Review B*, 75:94419

IV Björkman, T., Lizárraga, R., Bultmark, F., Eriksson, O., Wills, J., M., Bergman, A., Andersson, P. H. and Nordström, L. (2009) Studies of the incommensurate magnetic structure of a heavy fermion system: $CeRhIn_5$ *Submitted to Physical Review B*

V Hudl, M., Nordblad, P., Björkman, T., Eriksson, O., Häggström, L., Sahlberg, M., Vitos, L. and Andersson, Y. (2009) Order-disorder induced magnetic structures of $FeMnP_{0.75}Si_{0.25}$. *In Manuscript*

VI Souvatzis, P., Björkman, T., Eriksson, O., Andersson, P., Katsnelson, M. I. and Rudin, S. P. (2009) Dynamical stabilization of the body centered cubic phase in lanthanum and thorium by phonon-phonon interaction. *Journal of Physics: Condensed matter* 21:175402

VII Björkman, T. and Grånäs, O. Adaptive gaussian smearing for electronic structure calculations. (2009) *To be published in International Journal of Quantum Chemistry*

VIII Björkman, T., Eriksson, O. and Andersson, P. (2008) Coupling between the $4f$ core binding energy and the $5f$ valence band occupation of elemental Pu and Pu-based compounds. *Physical Review B*, 78:245101

Contents

1. Introduction

Most of our everyday experiences are determined by the electronic structure of materials. This might seem a strong statement, but nevertheless it is mostly true. The suns rays are of course powered by nuclear fusion processes, but when we feel their warmth on our skin it is because of the electronic structure of the nerve ends that register heat, and the electronic structure of the molecules of the atmosphere has ensured that wavelengths that would hurt us are mostly filtered out. The electronic structure of copper ensures that we have electricity in our homes, the electronic structure of the cooling medium makes it possible to transport heat out of the refrigerator and the electronic structure of a refrigerator magnet makes it stick to the fridge. And so on.

Of course we usually do not think of things like the feeling of heat on our skin in terms of electronic structure, and not even a refrigerator designer is likely to think very much about the electronic structure of the cooling medium. But in many technological applications as well as in fundamental research an understanding of electronic structures is absolutely essential.

This thesis is concerned mainly with theoretical studies from first principles, or *ab initio* theory, a term describing that we attempt to perform the calculations without inputting any information other than what is contained in the Schrödinger equation and universal constants. The focus of the studies is the electronic structure of f-electron materials, that is, materials that have properties that are determined by valence f-electrons of their constituent atoms. The electronic structure of f-electron materials is often complex and this in turn gives rise to both complex crystal and magnetic structures. The main difficulty lies in the electron correlation, the way that each electron is affected by all electrons around it, often is particularly strong in f-electron compounds.

Density functional theory (DFT) has in the last decades become the method of choice for first principles studies of solids. The great benefit of DFT lies in its capability of treating electron correlation without explicit references to individual electrons; all interactions are represented by an approximate effective potential that is determined only by the total electron density. Virtually all such approximations in current use are based on the local density approximation (LDA), which consists of taking the known solution[1] to a homogenous electron gas and apply the potential locally as if the density was homogenous.

[1] Or, more precisely, a parametrisation which is known to be very good.

Extending this, we may add functions of gradients of the density and get a generalised gradient approximation (GGA).

Both LDA and GGA in many situations tend to underestimate the tendency of the f-electrons to form localised states on a specific atomic site, and yields solutions in which the f-electrons move quite freely through the crystal. There are several ways of dealing with this problem, and three of them has been employed in this work, namely the self-interaction correction (SIC), the LDA+U method and the open core approximation.

When organising the material in this thesis the first comprehensive summary part has been put in the most natural order of theoretical progression. The papers, however, are ordered more thematically, the first two about a new implementation of the SIC method, then three studies of magnetic properties of materials, one on its own concerning lattice stability and the last two being concerned with evaluating and improving the precision of the calculational schemes. Sections briefly describing the papers will appear wherever their most natural place seemed to be.

2. Self-consistent field equations and the electronic structure of solids

2.1 Preliminary considerations

Before presenting the results of this thesis we need to look into some results of solid state physics that will be useful to us later on. This is not an overview or even an introduction to the whole field of solid state physics, but merely a brief statement of certain formulas which will later be referred to. For a full account the reader is referred to one of the many textbooks on the subject[40, 8, 29].

2.1.1 Electronic states in solids

A perfect solid is built up by an array of atoms in a periodic arrangement on a so-called Bravais lattice. In three dimensions it may be viewed as consisting of all points, $\mathbf{R}$, such that

$$\mathbf{R} = n_1\mathbf{a}_1 + n_2\mathbf{a}_2 + n_3\mathbf{a}_3, \tag{2.1}$$

where the $\{n_i\}_{i=1}^3$ are integers and the vectors $\{\mathbf{a}_i\}_{i=1}^3$ are primitive translation vectors of the lattice. These vectors are the smallest distance one needs to go along some direction before the lattice looks exactly the same. This translational symmetry puts certain constrains on the electronic wave functions, they must be of the Bloch form. This is most easily stated as the requirement that for each lattice site, $\mathbf{R}$, the electronic eigenstates must satisfy,

$$\psi(\mathbf{r} + \mathbf{R}) = e^{i\mathbf{k}\cdot\mathbf{R}}\psi(\mathbf{r}) \tag{2.2}$$

for some $\mathbf{k}$. A useful form for such functions may be obtained from functions centred on the atomic sites of the Bravais lattice,

$$\psi_{\mathbf{k}}(\mathbf{r}) = \sum_{\mathbf{R}} e^{i\mathbf{k}\cdot\mathbf{R}}\phi(\mathbf{r} - \mathbf{R}). \tag{2.3}$$

This is a sort of Fourier transform to a representation as a function of $\mathbf{k}$, and our description has been expanded into $\mathbf{k}$-space, where the functions are also periodic and described on the reciprocal lattice. Applying periodic — Born-von Karman — boundary condition to the Bloch wavefunction (2.2),

$$\psi(\mathbf{r} + n_i\mathbf{a}_i) = \psi(\mathbf{r}), \quad i = 1, 2, 3, \tag{2.4}$$

will make the wavefunction have the periodicity of the lattice. The wavefunction will also be periodic in $\mathbf{k}$-space, with a repeating cell that is typically taken to be the first Brillouin zone of the lattice[8]. This means that to describe the full solid, extending throughout all of space, we may restrict our attention to small volumes in both real space — the unit cell of the Bravais lattice — and in $\mathbf{k}$-space — the Brillouin zone.

2.1.2 The many-body problem in solids

With the problem of calculating the electronic structure of the a solid reduced to a small cell in space, and a similarly small volume in reciprocal space, we can turn to the problem of calculating the properties of the electrons in such a cell. This is a much more tractable number, as in crystalline solids a unit cell rarely has more than 100 atoms. With the number of valence electrons per atom being on the order of 10, this would mean that we typically do not need to worry about more than around 1000 electrons, a significantly more tractable number than the 10^{26} we started out with.

The problem is described by the Hamiltonian[1],

$$\begin{aligned} H &= T^N + V^{NN} + V^{Ne} + T^e + V^{ee} \\ &= \sum_i^N -\frac{1}{2M_i}\nabla^2_{\mathbf{R}_i} + \frac{1}{2}\sum_i^N\sum_{j\neq i}^N \frac{Z_i Z_j}{|\mathbf{R}_i - \mathbf{R}_j|} + \sum_i^N\sum_j^n \frac{Z_i}{|\mathbf{R}_i - \mathbf{r}_j|} \\ &\quad + \sum_i^n -\frac{\nabla^2_{\mathbf{r}_i}}{2} + \frac{1}{2}\sum_i^n\sum_{j\neq i}^n \frac{1}{|\mathbf{r}_i - \mathbf{r}_j|}, \end{aligned} \tag{2.5}$$

with sums taken over all nuclei (upper case letters) and electrons (lower case letters) in the unit cell.

The contributions to the energy are the kinetic and electrostatic energy of the nuclei, T^N and V^{NN}, the energy from electrostatic interactions between nuclei and electrons, V^{Ne}, the kinetic energy of the electrons, T^e, and the electron-electron interaction energy, V^{ee}.

We now simplify the problem even further by disregarding the motion of the nuclei, since they move very much slower than the electrons and their contribution to the Hamiltonian can therefore be treated separately from the dynamics of the electrons. We also for now disregard the nuclear-nuclear repulsion, which from the point of view of the electronic structure is just a constant. This constant is relevant for example if we wish to determine whether the crystal is stable. Integrating out the nuclear degrees of freedom in this way is known as the Born-Oppenheimer approximation.

[1] For notational convenience, Hartree atomic units will be used when describing the theory. To convert the formulas to Rydberg units, substitute $\frac{\nabla^2}{2} \to \nabla^2$ and multiply all electrostatic potentials by $e^2 = 2$.

There remains one reduction of the electronic system. The closed inner electronic shells of the atoms in a solid retain virtually all of their atomic character and will be treated in the calculations as if they were in a spherical potential with no possibility of moving around in the crystal. They are in principle still part of the many-body problem of the electrons, but since they are constrained to a single site their treatment is very simple. We may therefore think of all the remaining discussion in this chapter as pertaining to only the valence electrons.

What is now left is solving the quantum mechanical problem for the electrons in a single unit cell of the crystal. It consists of a number of interacting particles moving in an external potential, arising from the term V^{Ne}. Making the operators explicit, we write the Hamiltonian (omitting the superscript on the kinetic energy and renaming the Coulomb interaction between electrons U) as,

$$H = \hat{V}^{ext} + \hat{T} + \hat{U}. \tag{2.6}$$

The Schrödinger equation for the system of the electrons is now

$$\Bigg[\sum_{i}^{n}\left(-\frac{\nabla^2}{2} + V^{ext}(\mathbf{r})\right) + \sum_{\{i,j:i<j\}} U(\mathbf{r}_i,\mathbf{r}_j)\Bigg]\Psi(\mathbf{r}_1,\mathbf{r}_2,\ldots,\mathbf{r}_N) = E\Psi(\mathbf{r}_1,\mathbf{r}_2,\ldots,\mathbf{r}_N). \tag{2.7}$$

This equation is still a formidable problem, seeing as how the interacting many-body problem can only generally be solved for $N = 2$ and in some special cases for larger numbers. The general strategy of all electronic structure calculations is to replace the many-body interaction with some effective interaction.

2.2 The Hartree equations

One of the first attempts at an effective many-body theory for the electronic structure problem was the Hartree equation[30]. It can be seen as the simplest in a series of self-consistent field equations that will be outlined here.

The simplest way of constructing a many-body wavefunction is to simply write a product of normalised single particle wavefunctions, $\phi_i(\mathbf{r}_i)$,

$$\Psi(\mathbf{r}_1,\mathbf{r}_2,\ldots,\mathbf{r}_N) = \phi_1(\mathbf{r}_1)\phi_2(\mathbf{r}_2)\ldots\phi_N(\mathbf{r}_N). \tag{2.8}$$

Inserting this choice of wavefunction into equation (2.7) allows us to separate the problem for each electron and this leads to the Hartree equations,

$$\left(-\frac{\nabla^2}{2} + V^{ext}(\mathbf{r}) + V_i^H(\mathbf{r})\right)\phi_i(\mathbf{r}) = \epsilon_i\phi_i(\mathbf{r}), \tag{2.9}$$

where we have introduced the Hartree potential,

$$V_i^H(\mathbf{r}) = \sum_{j\neq i}\int d\mathbf{r}'\,\frac{\phi_j^*(\mathbf{r}')\phi_j(\mathbf{r}')}{|\mathbf{r}'-\mathbf{r}|} \tag{2.10}$$

that describes the electrostatic repulsion between the electrons. The summation is taken over all $j \neq i$ in order to ensure that an electron does not see contributions to the potential coming from itself. Exchanging the order of summation and integration in the above equation we have

$$\int d\mathbf{r}'\,\frac{\sum_{j\neq i}\phi_j^*(\mathbf{r}')\phi_j(\mathbf{r}')}{|\mathbf{r}'-\mathbf{r}|} = \int d\mathbf{r}'\,\frac{\rho_{N-i}(\mathbf{r}')}{|\mathbf{r}-\mathbf{r}'|}, \tag{2.11}$$

where it is readily seen that this just expresses the potential seen by electron i due to the average distribution of all other electrons, $\rho_{N-i}(\mathbf{r})$. We can also see that the wavefunctions will in general not be orthogonal to each other, since they all are solutions corresponding to different potentials.

2.3 The Hartree-Fock equations

According to the Pauli principle, the total wavefunction of any fermion system must be antisymmetric with respect to permutation of the particles. The Hartree wavefunction clearly does not satisfy this, as permutation of the single-particle orbitals leaves the wavefunction unchanged. To remedy this, we can use a different trial wavefunction, built up by antisymmetrizing the Hartree wavefunction. This is usually described by the construction of Slater determinants of the single-electron orbitals of equation (2.8)

$$\Psi(\mathbf{r}_1,\mathbf{r}_2,\ldots,\mathbf{r}_N) = \begin{vmatrix} \phi_1(\mathbf{r}_1) & \phi_1(\mathbf{r}_2) & \ldots & \phi_1(\mathbf{r}_N) \\ \phi_2(\mathbf{r}_1) & \phi_2(\mathbf{r}_2) & \ldots & \phi_2(\mathbf{r}_N) \\ \vdots & \vdots & \ddots & \vdots \\ \phi_N(\mathbf{r}_1) & \phi_N(\mathbf{r}_2) & \ldots & \phi_N(\mathbf{r}_N) \end{vmatrix}, \tag{2.12}$$

where the permutation of any two electrons will mean permutation of two rows (or columns) in the determinant, and so the wavefunction will have the

required antisymmetry. This results in the Hartree-Fock equations

$$\left(-\frac{\nabla^2}{2} + V^{ext}(\mathbf{r}) + V^H(\mathbf{r})\right)\phi_i(\mathbf{r}) + \int d\mathbf{r}'\, V^X(\mathbf{r}', \mathbf{r})\phi_i(\mathbf{r}) = \epsilon_i\phi_i(\mathbf{r}). \tag{2.13}$$

To note at this point are two important differences from the Hartree equations. Firstly, we have added the non-local exchange potential

$$V^X(\mathbf{r}', \mathbf{r}) = -\sum_j \frac{\phi_j^*(\mathbf{r}')\phi_j(\mathbf{r})}{|\mathbf{r}' - \mathbf{r}|} \tag{2.14}$$

that comes from the assumed antisymmetry of the wavefunction. It describes the effect that the electrons that come too close to each other are forced apart by the Pauli principle, two electrons cannot have the same quantum numbers, in particular, not occupy the same position in space. Secondly, we see that in the Hartree-Fock equations there are no restrictions on the summations over particles. The reason for this is that for $j = i$, the Hartree term and the exchange term will be identical, and so there is an orbital by orbital cancellation of any self-interaction.

2.4 Density functional theory and the Kohn-Sham equations

A completely different route to obtaining self-consistent field equations for the electronic problem is provided by density functional theory (DFT). As currently practised, DFT is implemented as an effective single-particle model that originates mainly from two sources, the work of Slater and co-workers with what was then known as the "X_α method"[59] which later got a firmer mathematical foundation in papers by Hohenberg and Kohn[35] and by Kohn and Sham[42]. Here will be outlined the canonical description of the theory as it can be derived from the Hohenberg-Kohn theorems.

The main idea behind DFT is to avoid the unpleasant problem of the very large number of interacting electrons by instead casting everything in terms of the electron density. No matter how complex our geometry or many electrons we put into our system the total density will always be described by only three spatial variables, so if we can succeed the simplification is clearly tremendous.

The starting point is to return to the many body Hamiltonian of Equation (2.6) acting on the space of all antisymmetric wavefunctions for the N-electron system, and to consider the following functional of the electron density in terms of the the kinetic energy and the electron-electron interaction,

$$F[n] = \min_{\psi \to n} \langle \psi | T + U | \psi \rangle. \tag{2.15}$$

The functional for the density, n, is defined as the minimum of the expectation value of the operator $T + U$ over all antisymmetric N-electron wavefunctions that produce that density. This property, to be a density corresponding to a N-electron wavefunction, is referred to as N-representability. The theorems were originally derived by considering densities generated by a potential, V-representable densities, but it turns out that not all N-representable densities are V-representable, so the current, more general, derivation is usually preferred nowadays. In terms of the functional (2.15) the Hohenberg-Kohn theorems can be stated.

Hohenberg-Kohn 1

$$E[n] = \int d\mathbf{r}\, V^{ext}(\mathbf{r}) n(\mathbf{r}) + F[n] \geq E_0 \tag{2.16}$$

where E_0 is the ground state energy of the system.

This establishes a variational principle for the functional E, which states that any trial density from the space of antisymmetric N-electron wavefunctions will always have an energy equal to or higher than the ground state energy of the interacting electron system.

Hohenberg-Kohn 2

$$E[n_0] = \int d\mathbf{r}\, V^{ext}(\mathbf{r}) n_0(\mathbf{r}) + F[n_0] = E_0 \tag{2.17}$$

The second theorem states that the value of the functional E evaluated for the true ground state of the interacting electron system is in fact equal to the ground state energy. A consequence of this is that a wavefunction of equation (2.15) that minimise $F[n_0]$ is the ground state wavefunction[2], and any ground state property can in principle be calculated as the expectation value of an operator with respect to this function. In other words *any* ground state property can be considered a functional of only the ground state density. These functionals are of course not known explicitly, but the result nevertheless gives us a handy door out from the world of N-body wavefunctions.

If suitable approximations to the terms T and U of the functional F were known we could now proceed to directly minimise the total energy functional, E, by fast and efficient means. Unfortunately, good approximations of this kind currently does not exist, and so progress must instead be made by some other means. In particular the kinetic energy functional, T, has resisted all attempts of accurate description. To handle this problem, Kohn and Sham derived equations by the following rearrangement of the terms in the interaction,

[2]We discuss here only non-degenerate ground states, but all results still hold for a degenerate ground state, with some minor modifications of the derivation.

$$T[n] + U[n] = T_S[n] + T'[n] + E^H[n] + E'[n]. \tag{2.18}$$

Here $T_S[n]$ is the kinetic energy of a system of non-interacting particles of density n, $E^H[n] = \int d\mathbf{r}\, V^H(\mathbf{r})n(\mathbf{r})$ is the Hartree energy and T' and E' are the remaining contributions coming from various many-body effects. This is a useful partitioning, since by far the largest part of the kinetic energy comes from the single particle contributions and the Hartree term takes care of most of the electron-electron interaction. We then lump together the primed quantities in a single term called the "exchange-correlation" which we will then try to find appropriate approximations for. The energy functional is now

$$E[n(\mathbf{r})] = T_S[n(\mathbf{r})] + \int d\mathbf{r}\, V^{ext}(\mathbf{r})n(\mathbf{r}) + E^H[n(\mathbf{r})] + E^{XC}[n(\mathbf{r})], \tag{2.19}$$

which at first may not seem like a great improvement over Equation (2.16). However, by considering the kinetic energy of only a non-interacting system, a solution presents itself, since we may then use some normalised single-particle wavefunctions, $\psi_i(\mathbf{r})$ such that $n(\mathbf{r}) = \sum_i \psi_i^*(\mathbf{r})\psi_i(\mathbf{r})$, and the single-particle part of the kinetic energy may be evaluated as

$$T_S[n(\mathbf{r})] = \sum_i \langle\psi_i(\mathbf{r})| -\frac{\nabla^2}{2}|\psi_i(\mathbf{r})\rangle. \tag{2.20}$$

For the ground state, the energy in Equation (2.19) is stationary with respect to variations in the density by the first Hohenberg-Kohn theorem. The most straightforward way to make this optimisation is to introduce a set of Lagrange multipliers, ϵ_i, to account for the constraint,

$$\langle\psi_i(\mathbf{r})|\psi_i(\mathbf{r})\rangle = 1. \tag{2.21}$$

We can then compute the functional gradient, $\nabla_{\langle\psi|}$, with respect to the set of orbitals and set the result equal to zero,

$$\nabla_{\langle\psi|}(E[n(\mathbf{r})] - \sum_i (\epsilon_i\langle\psi_i(\mathbf{r})|\psi_i(\mathbf{r})\rangle - 1)) = 0. \tag{2.22}$$

The effective single particle equations thus obtained are,

$$-\frac{\nabla^2}{2}|\psi_i(\mathbf{r})\rangle + \left(V^{ext}(\mathbf{r}) + \frac{\delta E^H[n(\mathbf{r})]}{\delta n(\mathbf{r})} + \frac{\delta E^{XC}[n(\mathbf{r})]}{\delta n(\mathbf{r})}\right)\frac{\delta n(\mathbf{r})}{\delta\langle\psi_i(\mathbf{r})|} =$$
$$\left(-\frac{\nabla^2}{2} + V^{ext}(\mathbf{r}) + V^H[n(\mathbf{r})] + V^{XC}[n(\mathbf{r})]\right)|\psi_i(\mathbf{r})\rangle = \epsilon_i|\psi_i(\mathbf{r})\rangle, \tag{2.23}$$

where we have used the definition of the Hartree energy from equation (2.13), and we have defined the exchange-correlation potential,

$$V^{XC}[n(\mathbf{r})] \equiv \frac{\delta E^{XC}[n(\mathbf{r})]}{\delta n(\mathbf{r})}. \tag{2.24}$$

These are the Kohn-Sham equations that have been extremely successful in the calculation of the properties of solids during the last decades.

Here it is important to note that when we introduced the wavefunctions ψ_i above, we made no assumptions about them other than that they are orthonormal. They are just some set of functions that when summed generate the electron density of the system. Furthermore, the parameters ϵ_i are just Lagrangian multipliers ensuring that the particle number is conserved. We often wish to identify the Kohn-Sham eigenvalues with quasi-particle eigenvalues, and differences between them as excitation energies. From the theory as so far derived here, however, there is no justification whatsoever for doing so. To obtain the correct quasi-particle spectrum we would need to solve an equation of the form[34],

$$\left(\frac{\nabla^2}{2} + V^{ext}(\mathbf{r}) + V^{H}(\mathbf{r})\right)\psi_i(\mathbf{r}) + \int d\mathbf{r}'\,\Sigma(\mathbf{r},\mathbf{r}',E_i)\psi_i(\mathbf{r}') = E_i\psi_i(\mathbf{r}), \tag{2.25}$$

where Σ is the quasi-particle self-energy. This equation is seductively similar to the Kohn-Sham equations, with the exchange-correlation potential replaced with the self-energy, but it is not true that the Kohn-Sham equations are simply an approximation to the more elaborate quasi-particle equation (2.25). The Kohn-Sham equations are capable of delivering the correct ground-state density and energy regardless of whether the quasi-particle self-energy can be approximated by a local and energy-independent quantity. Rather, the interpretation of the similarity between the equations is that *if* the self-energy can be approximated by a local, energy independent quantity, then we may interpret the Kohn-Sham spectrum as a quasi-particle spectrum as measured by for example an XPS experiment. While there is no simple way of knowing whether this holds in any particular situation, it is known that a Kohn-Sham spectrum usually gives a quite accurate picture of the true spectrum whenever strong correlations are not present.

2.4.1 Exchange-correlation functionals

The Kohn-Sham equations derive their usefulness from our ability to make sufficiently accurate approximations to the exchange-correlation energy and potential and an enormous amount of work has over the years gone into the design of new, and sometimes improved, functionals. We shall not attempt a complete description of any modern functional in current use, but instead say a few explanatory words on their most primitive origins.

The exchange-correlation functional is clearly a very complex object and had all our knowledge of the physics involved been the Kohn-Sham equations and their derivation there would be little hope of finding a suitable approximation. Progress is instead made possible by means of the Hartree-Fock theory. We can make a statistical approximation of the Hartree-Fock exchange energy, which by averaging removes the non-local character of the exchange potential (2.14). By regarding the homogenous electron gas, the eigenfunctions must by symmetry be plane waves, $e^{\pm ikr}$, occupied for all $k < k_F$, the Fermi k-vector. The resulting energy per particle from averaging the exchange over the whole Fermi sphere may be expressed

$$E^X = -\left(\frac{3}{\pi}\right)^{\frac{1}{3}} \int d\mathbf{r}\, n^{\frac{4}{3}}(\mathbf{r}) = -\left(\frac{3}{\pi}\right)^{\frac{1}{3}} \int d\mathbf{r}\, \epsilon^X[n(\mathbf{r})]n(\mathbf{r}), \qquad (2.26)$$

where in the last step we have introduced the quantity ϵ^X, interpreted as the exchange energy per particle and unit volume, the exchange energy density. Assuming that the density is sufficiently smooth, we might expect to get a good approximation to the exchange energy by simply evaluating this expression for the physical density at hand, and this is indeed found to be the case. If we account for the effects of correlation by a simple rescaling of the exchange by a factor α,

$$\epsilon^{XC}[n(br)] = \alpha\left(\frac{3}{\pi}\right)^{\frac{1}{3}} n^{\frac{1}{3}}(\mathbf{r}) \qquad (2.27)$$

and use this in the Kohn-Sham equations, we have the Slater X^α method[58, 59].

Equation (2.26) is the result of averaging over the whole Fermi sphere, but it is not obvious that this is in fact the correct method. The only electrons that really are "in position" to interact with one another are, unless the temperature is very high, the ones close to the Fermi surface. If the average is instead taken over only the surface of the Fermi sphere, the expression is,

$$\epsilon^X[n(\mathbf{r})] = \frac{3}{2}\left(\frac{3}{\pi}\right)^{\frac{1}{3}} n^{\frac{1}{3}}(\mathbf{r}). \qquad (2.28)$$

This expression was derived by Gaspar[23] and Kohn and Sham[42], and is the one that is used today. This form of the exchange energy is the basis for virtually all other approximations to the exchange-correlation energy. Typically, the partitioning between exchange and correlation is retained, and these parts are then described by fitting to suitable interpolation functions. Most of the raw data for these fits go back to quantum Monte Carlo simulations of the homogenous electron gas by Ceperley and Alder[14].

We list here some types of functionals that may be considered the most relevant for present-day use.

LDA - Local Density Approximations are the most direct extensions of the formula (2.28), typically built up by a rescaling of the exchange energy and one part coming from correlation. They have in common that they are local and not depending on gradients of the charge density.

GGA - Generalized Gradient Approximations are extensions to LDA that incorporate gradients of the density.

Hybrid functionals - A class of functionals of great importance in computational chemistry. It simply consists of mixing in some amount of the Hartree-Fock exchange energy in the functional and to evaluate this. Not often used in solid state applications, since they have the same disadvantages as the Hartree-Fock method itself for infinite systems.

Orbitally resolved corrections - A more important class of corrections for solid state applications that might be loosely described as ”spicing up” LDA with your favourite aspect of Hartree-Fock. They share the common characteristic that they are orbitally resolved and strive to restore some desirable property of the Hartree-Fock wavefunctions to the Kohn-Sham solutions. Examples include the self-interaction correction (SIC), LDA+U, exact exchange and orbital polarisation.

2.5 The self-consistent field procedure

With the introduction of density functional theory in the Kohn-Sham picture we have reduced the many-body problem to an effective one-particle problem. Still, there remains the Kohn-Sham equations to be solved, a coupled system of non-linear differential equations. We do this by means of the self-consistent field (SCF). If we can obtain some approximate initial potential, the Kohn-Sham equations will give approximate wavefunctions for that potential. If they are then squared to yield a density we can solve Poisson’s equation and an approximate exchange-correlation functional to construct a new potential, which can be reinserted into the Kohn-Sham equations and so on. When there is no longer any change in the density (or the potential, total energy or any other quantity of relevance) we have found a solution.

The starting point is to construct a suitable basis, expand the solutions in that to obtain a solution in terms of the expansion coefficients. The solution is usually sought in the form of wavefunctions directly or by means of Green’s functions, and the procedure will be slightly different depending on this choice. The wavefunction approach is most straightforward and with somewhat less practical difficulties in implementation, but the Green’s functions are a more general and powerful representation for further developments. Once the Kohn-Sham equations for a given potential are solved, the Fermi level must be determined. Then the scheme proceeds with computing the den-

sity and then, using that density, determine a new effective potential by solving Poissons equation for the solid. There are as many solutions to these different problems as there are electronic structure programmes, but these main steps are always the same:

1. Construct a basis.
2. Set up the Hamiltonian in this basis. Solve the eigenvalue problem (wave-function approach) or invert the Hamiltonian (Green's function approach).
3. Find the Fermi level.
4. Solve Poissons equation for the resulting density.
5. Evaluate the total energy.

To these may be added that we also need to provide some sort of starting guess for the effective potential. In this work several different methods for implementing the above scheme has been used, and we will now look into one of them, the full-potential linear muffin-tin orbital method, in detail.

2.6 Paper VI. Lattice vibrations in La and Th

The approximation that the lattice is static is not always sufficient, and to account for the movement of the atoms in a solid, the phonon spectrum may need to be calculated. That way the phonon contribution to the free energy can be calculated and phases that would otherwise be energetically unfavourable may be stabilised by the vibrations. However, the phonon picture of lattice vibrations is also an approximation, coming from the assumption that the atoms experience a force proportional to their displacement. When this assumption breaks down, what happens is that instead of a set of phonons, the quantisation of an independent set of harmonic oscillators, we must model the lattice vibrations as a set of *interacting* phonons.

In Paper VI we apply the self-consistent ab initio lattice dynamics (SCAILD) method[61, 62] to study two cases where the independent phonon approximation does not apply, the bcc phases of La and Th. If the phonon spectrum is calculated directly, imaginary frequencies will appear in the phonon spectrum, induced by the anharmonicity of the lattice. The study demonstrates that the phases are possible to stabilise if the phonon-phonon interaction is properly accounted for.

3. Full-potential LMTO

The linear muffin-tin orbital method, LMTO, is one of the most successful methods of computational materials science. It was developed by O. K. Andersen[3] as a computationally more efficient way of solving the Korringa-Kohn-Rostoker (KKR) equations. The method was originally devised to make use of the atomic sphere approximation (ASA), but is not restricted to geometric approximations, as long as the muffin-tin geometry is applicable. An excellent account of the original LMTO-ASA method has been given by H. L. Skriver[57].

Described here is the full-potential LMTO method as implemented in the software package RSPt[1] developed by Wills et al.[76] The aim of the description is to be a suitable introduction for someone interested in using this method, but who has no previous experience of LMTO theory. The notation is that used by Wills *et al*. in the main reference[76], and is largely similar to other references to the LMTO method[57, 4].

3.1 Crystal symmetry

In the following it will be convenient to introduce some slightly modified versions of the spherical harmonics[36], $Y_{\ell m}(\hat{\mathbf{r}})$,

$$\mathcal{Y}_{\ell m}(\hat{\mathbf{r}}) = i^{\ell} Y_{\ell m}(\hat{\mathbf{r}}) \tag{3.1a}$$

$$C_{\ell m}(\hat{\mathbf{r}}) = \sqrt{\frac{4\pi}{2\ell+1}} Y_{\ell m}(\hat{\mathbf{r}}) \tag{3.1b}$$

$$\mathcal{C}_{\ell m}(\hat{\mathbf{r}}) = i^{\ell} \sqrt{\frac{4\pi}{2\ell+1}} Y_{\ell m}(\hat{\mathbf{r}}). \tag{3.1c}$$

Here the angular variables, (θ, ϕ), are denoted by $\hat{\mathbf{r}}$. A related quantity is the Gaunt coefficient, the integral of the product of three spherical harmonics, here in two slightly different forms

$$G(\ell, m; \ell', m'; \ell'', m'') = \int d\hat{\mathbf{r}}\, Y_{\ell m}(\hat{\mathbf{r}}) Y^*_{\ell' m'}(\hat{\mathbf{r}}) Y_{\ell'' m''}(\hat{\mathbf{r}}) \tag{3.2}$$

$$\mathcal{G}(\ell, m; \ell', m'; \ell'', m'') = \int d\hat{\mathbf{r}}\, \mathcal{Y}_{\ell m}(\hat{\mathbf{r}}) \mathcal{Y}^*_{\ell' m'}(\hat{\mathbf{r}}) \mathcal{C}_{\ell'' m''}(\hat{\mathbf{r}}). \tag{3.3}$$

Any function of the three spatial dimensions can locally on an atomic site, $\boldsymbol{\tau}$, be expressed in spherical polar coordinates with the angular part expanded in spherical harmonics. Due to the symmetry of the lattice only specific linear combinations of spherical harmonics will contribute, and each such linear combination is common to all equivalent atomic sites of the Bravais lattice. To decrease the cost of computations, we therefore express things in these linear combinations, $D_{ht}(\hat{\mathbf{r}})$, and change the indexing from site, $\boldsymbol{\tau}$, to type, t, where every type can have several equivalent site as its members. We also introduce the operator $\mathcal{D}_{\boldsymbol{\tau}}$, that rotates the coordinates of its argument into the coordinates of the desired site, $\boldsymbol{\tau}$. Assuming only purely rotational symmetry types are present, this operator is simply a rotation matrix expressing a rotation of the local coordinate system, possibly in combination with the inversion operation.

In formulas we have for a symmetric function at a site, $\boldsymbol{\tau}$,

$$f(\mathbf{r})|_{\boldsymbol{\tau}} = \sum_{\ell=0}^{\ell_{max}} \sum_{m=-\ell}^{\ell} f_{\boldsymbol{\tau},\ell m}(r) Y_{\ell m}(\hat{\mathbf{r}}) = \tag{3.4a}$$

$$f(\mathcal{D}_{\boldsymbol{\tau}}\mathbf{r}_{\boldsymbol{\tau}})|_t = \sum_h f_{ht}(r) D_{ht}(\mathcal{D}_{\boldsymbol{\tau}}\hat{\mathbf{r}}_{\boldsymbol{\tau}}). \tag{3.4b}$$

The variable $\mathbf{r}_{\boldsymbol{\tau}}$ signals that the formula is in a coordinate system local to the site, that is, with its origin on that site. These equations should be read as follows: "The symmetric function, f, on the site $\boldsymbol{\tau}$ is a linear combination of spherical harmonics times a radial function, which is obtained by a rotation of a linear combination of symmetrised harmonic functions around the type, t."

The symmetrised harmonic functions, calculated beforehand, are built up from spherical harmonics using the symmetry coefficients, $\alpha_{ht}(m)$, and a spherical harmonic, $\mathcal{C}_{\ell m}(\hat{\mathbf{r}})$,

$$D_{ht}(\hat{\mathbf{r}}) = \sum_m \alpha_{ht}(m) \mathcal{C}_{\ell_h m}(\hat{\mathbf{r}}). \tag{3.5}$$

3.2 Basis functions

While there is no geometrical restrictions on the shape of the potential in FP-LMTO, the basis functions are still taken to be the same as in the LMTO-ASA method[57]. The lattice is described by a partitioning in spherical regions around the atomic sites called muffin-tins and in between them the interstitial region. We may think of it as a set of atomic-like regions – the muffin-tins – dispersed in a free-electron-like interstitial "sea". The basis, and consequently all other quantities, are defined through this partitioning of space. The LMTO method constructs a set of basis functions centred on each lattice site, but the geometry is the same in the APW methods, but there the starting point for the

basis is instead plane waves. These interstitial functions are often referred to as the envelope functions of the basis.

Once the basis is constructed we construct and solve the generalised eigenvalue problem,

$$(\mathcal{H} - \mathcal{O}\epsilon)\,\mathcal{A} = 0 \tag{3.6}$$

where ϵ and $\mathcal{A}$ are eigenvalues and eigenvectors respectively, and $\mathcal{H}$ and $\mathcal{O}$ are the full-potential Hamiltonian and overlap matrices.

3.2.1 The basis in the interstitial

We start by setting up a basis for the interstitial region, consisting of functions centred on each atomic site. Since the potential in this region is fairly flat, the most obvious choice are free-electron solutions. In spherical coordinates these are spherical Bessel and Neumann functions, j_ℓ and n_ℓ, times an angular part that are the spherical harmonic functions of Equation (3.1a). Explicitly,

$$N_{\ell m}(\kappa, \mathbf{r}) = n_\ell(\kappa r)\mathcal{Y}_{\ell m}(\hat{\mathbf{r}}) \tag{3.7}$$

$$J_{\ell m}(\kappa, \mathbf{r}) = j_\ell(\kappa r)\mathcal{Y}_{\ell m}(\hat{\mathbf{r}}), \tag{3.8}$$

if the centre of the site is taken to be at the origin. The κ quantum number is a measure of the kinetic energy, just like the wavenumber, k, in the free-electron problem in Cartesian coordinates.

The basis functions will be used to calculate quantities such as the overlap, $\langle\psi_i|\psi_j\rangle$, and Hamiltonian matrix elements, $\langle\psi_i(\mathbf{r})|H|\psi_j(\mathbf{r})\rangle$, and since the basis functions i and j will in general be centred on different atoms, they are examples of so-called two-centre integrals. The LMTO formalism reduces these to one-centre integrals by means of an expansion theorem, which states that a function of the type (3.7) centred at a site, $\boldsymbol{\tau}_1$ may be expanded around any other site, $\boldsymbol{\tau}_2$ using the following relation

$$N_{\ell m}(\kappa, \mathbf{r} - \boldsymbol{\tau}_1) = 4\pi \sum_{\ell' m'} \sum_{\ell'' m''} G(\ell, m; \ell', m'; \ell'', m'') \times N^*_{\ell'' m''}(\kappa, \boldsymbol{\tau}_1 - \boldsymbol{\tau}_2) J_{\ell' m'}(\kappa, \mathbf{r} - \boldsymbol{\tau}_2). \tag{3.9}$$

For our interstitial basis we choose the following linear combinations of partial waves,

$$\mathcal{K}_{\ell m}(\kappa, r) = -\kappa^{\ell+1} \begin{cases} N_{\ell m}(\kappa, r) - iJ_{\ell m}(\kappa, r) & \kappa^2 < 0, \\ N_{\ell m}(\kappa, r) & \kappa^2 > 0, \end{cases} \tag{3.10}$$

and for future reference also introduce

$$\mathcal{J}_{\ell m}(\kappa, r) = \kappa^{-\ell} J_{\ell m}(\kappa, r). \tag{3.11}$$

We note that in the $\kappa^2 < 0$ case the basis function in (3.10) is the spherical Hankel function, $iH^+_{\ell m}(\kappa, r)$. Essentially the form of Equation (3.10) is made to get a suitably short ranged orbital[57]. We also mention here that the parameter, κ, is chosen by us as one of the parameters that specify our basis, and we will return to a more thorough discussion of how to choose these in Chapter 3.7.1.

Using the basis function of Equation (3.10) to build Bloch orbitals, we get the basis function, labelled by i,

$$\begin{aligned}\psi_i(\mathbf{k},\mathbf{r}) &= \sum_{\mathbf{R}} e^{i\mathbf{k}\cdot\mathbf{R}}\mathcal{K}_{\ell_i m_i}(\kappa_i, \mathcal{D}_{\boldsymbol{\tau}_i}(\mathbf{r}-\boldsymbol{\tau}_i-\mathbf{R})) \\ &= \mathcal{K}_{\ell_i m_i}(\kappa_i, \mathcal{D}_{\boldsymbol{\tau}_i}(\mathbf{r}-\boldsymbol{\tau}_i))\delta(\boldsymbol{\tau},\boldsymbol{\tau}_i) + \sum_{\mathbf{R}\neq 0} e^{i\mathbf{k}\cdot\mathbf{R}}\mathcal{K}_{\ell_i m_i}(\kappa_i, \mathcal{D}_{\boldsymbol{\tau}_i}(\mathbf{r}-\boldsymbol{\tau}_i-\mathbf{R})).\end{aligned} \tag{3.12}$$

The first row is the defining expression for a basis function in the interstitial region. In the second row, we split the summation over sites in the term from $\boldsymbol{\tau}_i$ and the rest. This is to get a more convenient form for the basis function also inside the other muffin tins. To reduce the amount of notation we for a moment constrain ourselves to the case $\kappa^2 > 0$, and combine this with the expansion (3.9), we get for the basis function, i, the following expression, evaluated at the site $\boldsymbol{\tau}$,

$$\begin{aligned}\psi_i(\mathbf{k},\mathbf{r})\big|_{\boldsymbol{\tau}} &= \mathcal{K}_{\ell_i m_i}(\kappa_i, \mathcal{D}_{\boldsymbol{\tau}_i}(\mathbf{r}-\boldsymbol{\tau}_i))\delta(\boldsymbol{\tau},\boldsymbol{\tau}_i) + \sum_{\ell m}\mathcal{J}_{\ell m}(\kappa_i, \mathcal{D}_{\boldsymbol{\tau}}(\mathbf{r}-\boldsymbol{\tau})) \\ &\times 4\pi\sum_{\mathbf{R}\neq\boldsymbol{\tau}_i} e^{i\mathbf{k}\cdot\mathbf{R}}\sum_{\ell',m'}\kappa^{\ell+\ell_i-\ell'}G(\ell,m;\ell_i,m_i;\ell',m')N^*_{\ell' m'}(\kappa_i,\boldsymbol{\tau}-\boldsymbol{\tau}_i-\mathbf{R}) \\ &= \mathcal{K}_{\ell_i m_i}(\kappa_i, \mathcal{D}_{\boldsymbol{\tau}_i}(\mathbf{r}-\boldsymbol{\tau}_i))\delta(\boldsymbol{\tau},\boldsymbol{\tau}_i) \\ &\quad + \sum_{\ell m}\mathcal{J}_{\ell m}(\kappa_i, \mathcal{D}_{\boldsymbol{\tau}}(\mathbf{r}-\boldsymbol{\tau}))B_{\ell m;\ell_i m_i}(\kappa_i,\boldsymbol{\tau}-\boldsymbol{\tau}_i,\mathbf{k}).\end{aligned} \tag{3.13}$$

We have here introduced the *structure constants* or *structure functions*, $B_{\ell m;\ell' m'}(\kappa,\boldsymbol{\tau}-\boldsymbol{\tau}',\mathbf{k})$, and remind ourselves that this particular expression is valid for $\kappa^2 > 0$. For $\kappa^2 < 0$ we have a Hankel function instead of a Neumann function, and the structure constant is given by an analogous expression for this case[1].

At this point it is suitable to make a few more general remarks. The expression in Equation (3.13) expresses the behaviour of a basis function centred at $\boldsymbol{\tau}_i$ around the its own site, and site around any other site, $\boldsymbol{\tau}$. This is a *two-centre expansion* of the wavefunction, the two centres being $\boldsymbol{\tau}_i$ and $\boldsymbol{\tau}$. As will be seen, this can be used to reduce two-centre integrals to sums over one-centre integrals.

[1] For the Hankel function this gives the structure constants used in KKR theory[78].

Much work has been done in relation to the expression (3.13) in other developments of MTO theory. By modelling some form of response at all other sites to the presence of a wavefunction at $\boldsymbol{\tau}$, the expression in Equation (3.13) can be "rebalanced" in such a way that the contributions on other sites becomes much smaller. The expressions corresponding to (3.13) are then said to be written in a screened representation, using the screened structure constants. By these means we may construct a more short-ranged representation where the basis functions do not extend throughout all space, but vanishes after a couple, or even just one, neighbouring shells. These approaches started with the introduction of tight-binding (TB) LMTO[5] and has since given rise to a long list of methods like the third-generation LMTO[4], EMTO[72] and screened KKR[79].

3.2.2 The basis in the muffin-tins

With a basis in the interstitial constructed, we move on to improving on it inside the muffin-tins. A basis made up purely from Bessel, Neumann and Hankel functions would end up in the same problem as a plane-wave basis, namely that the total wavefunction is not very well-behaved near the atomic nuclei, and we would need a very large basis to deal with them. So we move on by *augmenting* the basis. This simply means to hack off a bit and replace it with something else, in the case of LMTO, we exchange the basis inside the muffin-tins for a local solution to the Schrödinger equation for a spherical potential at a representative energy[2],

$$\left(-\frac{d^2}{dr^2}+\frac{\ell(\ell+1)}{r^2}+V_{MT}(r)-E_\ell\right) r\,\phi_\ell(E_\ell,r)=0. \tag{3.14}$$

This is solved on a logarithmic mesh using standard numerical methods[47]. Note that this is not an eigenvalue equation, we impose no boundary condition and the energy is not something that is being sought, but a number dictated by us. We may picture that we "probe" the system at an energy E_ℓ to find a suitable guess for trial wavefunction.

In order to create a basis function that is good for a range of energies around E_ℓ, we also compute the energy derivative of the function ϕ_ℓ,

$$\dot{\phi}_\ell(E_\nu,r)=\left.\frac{\partial\phi(E,r)}{\partial E}\right|_{E=E_\nu}. \tag{3.15}$$

We will now make linear combinations of the functions $\phi_\ell(r)$ and $\dot{\phi}_\ell(r)$, and may think of it as a Taylor expansion of the energy dependence around the energy E_ν for the ℓ shell. The linear combination we choose, should be such

[2]What is solved is not in fact the Schrödinger equation, but the scalar relativistic equation of Koelling and Harmon[41], but this distinction is not important for present purposes.

that the basis is continuous and differentiable everywhere, in particular across the muffin-tin boundary, which means that we also need to specify the linear combination of radial derivatives, $\phi'_\ell(r)$ and $\dot{\phi}'_\ell(r)$. If we now regard the one-centre expansion (3.13) evaluated at the muffin-tin boundary of the type t, for each $\mathbf{k}$-point, and match the corresponding ℓ components of the envelope functions and our local atomic solutions, we get the required matching criterion, here expressed in matrix form[3],

$$\begin{pmatrix} \phi_\ell(E_\nu, S_t) & \dot{\phi}_\ell(E_\nu, S_t) \\ \phi'_\ell(E_\nu, S_t) & \dot{\phi}'_\ell(E_\nu, S_t) \end{pmatrix} \begin{pmatrix} \omega_1^h(E_\nu, \kappa) & \omega_1^j(E_\nu, \kappa) \\ \omega_2^h(E_\nu, \kappa) & \omega_2^j(E_\nu, \kappa) \end{pmatrix} = \begin{pmatrix} \mathcal{K}_\ell(\kappa, S_t) & \mathcal{J}_\ell(\kappa, S_t) \\ \mathcal{K}'_\ell(\kappa, S_t) & \mathcal{J}'_\ell(\kappa, S_t) \end{pmatrix}. \quad (3.16)$$

Once the ω coefficients are determined we have the basis functions in the muffin-tins as,

$$\psi_i(\mathbf{k}, \mathbf{r}) = \psi^{(1)}_{t_i;\ell_i m_i}(E_{t;\ell}, \mathbf{r})\delta(\boldsymbol{\tau}-\boldsymbol{\tau}_i)+\sum_{\ell m} \psi^{(2)}_{t;\ell m}(E_{t;\ell}, \mathbf{r}) B_{\ell m;\ell_i m_i}(\kappa_i, \boldsymbol{\tau}-\boldsymbol{\tau}_i, \mathbf{k}), \quad (3.17)$$

with,

$$\begin{aligned} \psi^{(1)}_{t;\ell m}(E_{t;\ell}, \mathbf{r}) =& (\phi_{t;\ell m}(E_{t;\ell}, r)\omega_1^h(E_{t;\ell}, \kappa) \\ &+ \dot{\phi}_{t;\ell m}(E_{t;\ell}, r)\omega_2^h(E_{t;\ell}, \kappa))\mathcal{Y}_{\ell m}(\hat{\mathbf{r}}) \end{aligned} \quad (3.18)$$

$$\begin{aligned} \psi^{(2)}_{t;\ell m}(E_{t;\ell}, \mathbf{r}) =& (\phi_{t;\ell m}(E_{t;\ell}, r)\omega_1^j(E_{t;\ell}, \kappa) \\ &+ \dot{\phi}_{t;\ell m}(E_{t;\ell}, r)\omega_2^j(E_{t;\ell}, \kappa))\mathcal{Y}_{\ell m}(\hat{\mathbf{r}}) \end{aligned}. \quad (3.19)$$

Note that we in expression (3.17) still has the same split in a parent contribution, here given the index 1, and a second contribution consisting of a structure function summation. In some applications, most notably the dynamical mean field theory (DMFT) implementation in the present FP-LMTO scheme, the ϕ term of (3.18) is termed the "head" of the muffin-tin. It turns out that the tails coming in from other functions will be the main contribution to the $\dot{\phi}$ terms of the expansion, and it is often useful to think of the muffin-tin orbital, in its own muffin-tin, as an essentially atomic-like state that near the muffin-tin boundary is modified by the tails of atomic-like states centred on all other sites[4]. A pictorial representation of the muffin-tin orbital is given in Figure 3.1.

In heavier elements, the highest core states will be so delocalised that they start to form bands. These bands, isolated in energy from the rest of the valence band and so hybridise very little with other electrons, are referred to as

[3]The somewhat idiosyncratic indexing of the expansion coefficients, ω, comes from an attempt here to conform to naming conventions used in the source code of the RSPt program.

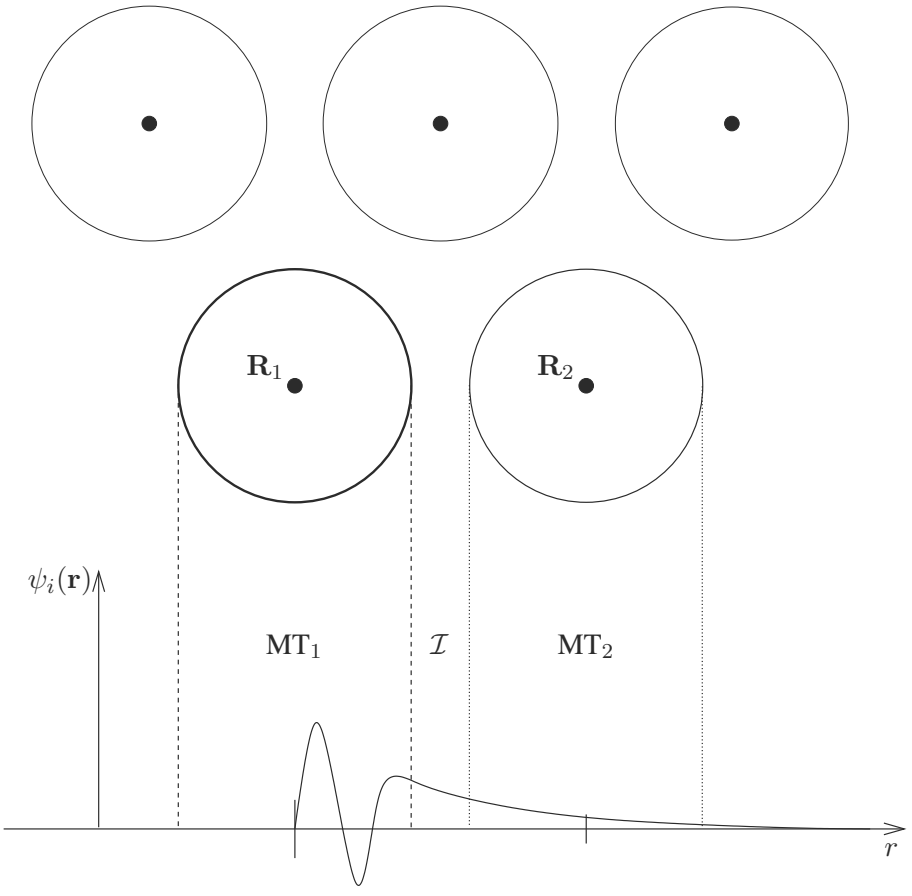

Figure 3.1: The LMTO geometry. The upper part of the figure shows an array of spherical regions, "muffin-tins", centred on the lattice sites, and the interstitial region. The lower part shows the form of a basis function along the line connecting the two spheres at $\mathbf{R}_1$ and $\mathbf{R}_2$. In the region MT_1, the muffin-tin centred at $\mathbf{R}_1$, the basis function is given by Equation (3.18), in region MT_2 it is given by the ℓm sum of Equation (3.17). In the interstitial region, $\mathcal{I}$, the basis function is given by Equation (3.10).

semi-core states. In order to fully describe the solid, the basis needs to include also these states of similar ℓ value but different principal quantum number from the valence states. This is easily accomplished by simply assigning different linearisation energies to the different states. Basis functions with the same ℓ values but different values of $E_{t;\ell}$ are said to belong to different energy sets.

We have yet to choose appropriate values for the linearisation energies, $E_{t;\ell}$. The preferred way in the FP-LMTO method is to self-consistently minimise the total energy with to respect them, and this is clearly always justifiable since the aim of the SCF scheme is to minimise the total energy.[4] When this method is applied with multiple basis energy sets we also run a risk that the semi-core and valence basis functions will start to mix and produce a non-physical basis. The preferred way to avoid this to employ the same procedure as was originally used to ensure the orthogonality of the core states to the valence states[57] and take the valence function to have the same logarithmic derivative at the muffin-tin boundary as the semi-core function, but one node more. This ensures that they are orthogonal to each other, and will keep the linearisation energies apart.

We will end this section by a change of notation to simplify later sections and to conform to the convention of the original reference of the method[76]. We will introduce a vector notation such that the basis function in Equation (3.17) can be written as

$$\psi_i(\mathbf{k},\mathbf{r}) = \sum_{\ell m} \mathrm{U}_{t;\ell m}(e_i, \mathcal{D}_{\boldsymbol{\tau}}\mathbf{r}_t)\Omega_{t\ell}(e_i,\kappa_i)\mathrm{S}_{\ell m;\ell_i m_i}(\kappa_i, \boldsymbol{\tau}-\boldsymbol{\tau}_i, \mathbf{k}). \quad (3.20)$$

Here Ω is the 2×2 matrix of the ω's in Equation (3.16), and

$$\mathrm{U}(e_i,\mathbf{r}) = \big(\phi(e_i,\mathbf{r}), \dot{\phi}(e_i,\mathbf{r})\big), \quad (3.21)$$

$$\mathrm{S}_{\ell m;\ell' m'}(\kappa, \boldsymbol{\tau}-\boldsymbol{\tau}', \mathbf{k}) = \begin{pmatrix} \delta(\boldsymbol{\tau},\boldsymbol{\tau}')\delta(\ell,\ell')\delta(m,m') \\ B_{\ell m;\ell' m'}(\kappa, \boldsymbol{\tau}-\boldsymbol{\tau}', \mathbf{k}) \end{pmatrix}. \quad (3.22)$$

The symbol e_i denotes the linearisation energy of basis function i. We also need

$$\mathrm{K}_\ell(\kappa, r) = \big(\mathcal{K}_\ell(\kappa,r), \mathcal{J}_\ell(\kappa,r)\big). \quad (3.23)$$

3.3 Interstitial quantities

Since we chose the basis functions in the interstitial region to be eigenfunctions of the kinetic energy operator, the kinetic energy matrix elements are

[4] Historically the LMTO method has typically been used in the atomic sphere approximation (ASA) and as a minimal basis. In this case the parameters must sometimes be chosen differently depending on the property to be calculated[57].

easily evaluated as simply,

$$\langle\psi_i| - \nabla^2|\psi_j\rangle = \frac{1}{2}(\kappa_i^2 + \kappa_j^2)\langle\psi_i|\psi_j\rangle, \tag{3.24}$$

whence,

$$\langle\psi_i|\psi_j\rangle = -(\kappa_j^2 - \kappa_i^2)^{-1}\int_I d\mathbf{r}\,(\psi_i^\dagger(\mathbf{r})(\nabla^2\psi_j(\mathbf{r})) - (\nabla^2\psi_i^\dagger(\mathbf{r}))\psi_j(\mathbf{r})). \tag{3.25}$$

Written in this form we may rewrite the overlap using Green's identity to reshape the integration over the interstitial volume into an integral involving radial derivatives of the basis functions over the interstitial surface (i.e. the surfaces of the muffin-tin spheres). Using the Wronskian, $W(f,g) = f\frac{\partial g}{\partial r} - \frac{\partial f}{\partial r}g$, we get

$$\begin{aligned}
&\langle\psi_i(\mathbf{r},\mathbf{k})|\psi_j(\mathbf{r},\mathbf{k})\rangle = \\
&(\kappa_j^2 - \kappa_i^2)^{-1}\sum_{\boldsymbol{\tau}} S_t^2\int_I \hat{\mathbf{r}}\,W(\psi_i^\dagger,\psi_j) = \sum_{\boldsymbol{\tau}} S_t^2\sum_{\ell,m}\mathrm{S}^\dagger_{\ell m;\ell_i m_i}(\kappa_i,\boldsymbol{\tau}-\boldsymbol{\tau}_i,\mathbf{k}) \\
&\qquad\times\frac{W(\mathbf{K}_\ell^\dagger(\kappa_i,S_t),\mathbf{K}_\ell(\kappa_j,S_t))}{\kappa_j^2-\kappa_i^2}\mathrm{S}^\dagger_{\ell m;\ell_i m_i}(\kappa_i,\boldsymbol{\tau}-\boldsymbol{\tau}_i,\mathbf{k})
\end{aligned} \tag{3.26}$$

The evaluation of the potential matrix elements follows a more elaborate procedure. This is so, since by simply squaring the eigenvectors and use the definition of the basis function over the interstitial we would have a representation of the density that is cumbersome to use for solving Poissons equation. What we instead want is to represent these quantities in reciprocal space as a Fourier series since it is then a trivial matter to write down the potential. Straightforward Fourier transformation of the basis functions and densities is not feasible, however, because of the oscillatory behaviour inside the muffin-tins, which would make the series too poorly convergent. This obstacle must clearly be avoidable, since we are only interested in the values of these quantities in the interstitial region, and there basis functions and densities are smooth. What is needed is the construction of pseudo-quantities that are equal to the true quantities in the interstitial and are smooth functions inside the muffin-tins, which retain just enough of the real characteristics to be able to match smoothly to the interstitial.

For the pseudo potential constructed in this way we have for the interstitial,

$$\langle\psi_i(\mathbf{r})|V(\mathbf{r})|\psi_j(\mathbf{r})\rangle\Big|_I = \langle\tilde{\psi}_i(\mathbf{r})|\theta_I\tilde{V}(\mathbf{r})|\tilde{\psi}_j(\mathbf{r})\rangle\Big|_{cell}, \tag{3.27}$$

where the pseudo wavefunctions and pseudo potential has added tildes and we have introduced the interstitial step function, θ_I which is zero inside the muffin-tins and 1 in the interstitial.

The pseudo potential has contributions from two parts, the pseudo density, $\tilde{n}(\mathbf{g})$, constructed by squaring the pseudo wavefunctions, $\tilde{\psi}(\mathbf{r},\mathbf{k})$ and and a second part, $\tilde{n}^{(p)}(\mathbf{r})$, defined within the muffin-tins to give the correct multipole moments.

The pseudo potential is given throughout the unit cell as,

$$\tilde{V}(\mathbf{r}) = 4\pi e^2 \sum_{\mathbf{g}\neq 0} \frac{\tilde{n}(\mathbf{g}) + \tilde{n}^{(p)}(\mathbf{g})}{g^2} e^{i\mathbf{g}\cdot\mathbf{r}}. \tag{3.28}$$

The construction of the pseudo quantities inside the muffin-tins along with the considerations leading to their definition are well described in the original reference[76] and references therein, and we will just briefly state them and give short descriptions of their content. The pseudo wavefunction inside the muffin tins is obtained as the solution to the equation,

$$(\nabla^2 + \kappa_i^2)\tilde{\psi}_i(\kappa_i,\mathbf{r}) = -c_\ell \left(\frac{r}{s}\right)^\ell \left[1 - \left(\frac{r}{s}\right)^2\right]^n \mathcal{Y}_{\ell m}(\hat{\mathbf{r}})\Theta(s-r), \tag{3.29}$$

and the pseudo density in the muffin-tins is given by,

$$\tilde{n}^{(p)}(\mathbf{r}) = \sum_{\boldsymbol{\tau}} \sum_h \tilde{n}_{ht}^{(p)}(r_{\boldsymbol{\tau}}) D_{ht}(\mathcal{D}_{\boldsymbol{\tau}}\hat{\mathbf{r}}_{\boldsymbol{\tau}}) \tag{3.30}$$

$$\tilde{n}_{ht}^{(p)}(r_{\boldsymbol{\tau}}) = c_{ht} \left(\frac{r}{s}\right)^\ell \left[1 - \left(\frac{r}{s}\right)^2\right]^n \Theta(s-r). \tag{3.31}$$

The coefficients c_ℓ of Equation (3.29) are determined so as to match the pseudo wavefunction to the true wavefunction, $\mathcal{K}_{\ell m}(\kappa,\mathbf{r})$ at the radius s, which must be smaller than or equal to the muffin-tin radius. The density coefficient c_{ht} of equation (3.31) are instead determined by the requirement, in terms of the true muffin-tin density, $n(\mathbf{r})$ and the squared pseudo wavefunctions,

$$\int_0^s d\mathbf{r}\, r_{\boldsymbol{\tau}}^\ell\, D_{ht}^*(\mathcal{D}_{\boldsymbol{\tau}}\hat{\mathbf{r}}_{\boldsymbol{\tau}})(\tilde{n}^{(p)}(\mathbf{r}) - n(\mathbf{r}) + \tilde{n}(\mathbf{r})) = 0. \tag{3.32}$$

The above equations also introduce the muffin-tin stepfunction, $\Theta(s_{\boldsymbol{\tau}} - r)$, which is 1 inside the muffin-tin centred at $\boldsymbol{\tau}$ and 0 elsewhere, and an exponent, n, which is arbitrary, but may be chosen to ensure that the pseudo quantities has sufficiently rapidly convergent Fourier series. By comparison of Equations (3.29) and (3.31) it is easy to see that the constructions of the two are related. The idea is in both cases to construct a function that has multipole moments that matches the true quantity. If in Equation (3.32) the term containing the true density is moved to the right hand side, we see that the requirement means that $\tilde{n}^{(p)}(\mathbf{r})$ forms a compensation charge inside the muffin-tins to ensure that the pseudo density gets the correct multipole moments.

3.4 Muffin-tin quantities

3.4.1 Matrix elements

For the muffin-tin part of the matrix elements, we split the Hamiltonian in a spherical part plus the non-spherical (or "full-potential") part,

$$\mathcal{H} = H_0 + v_{ht}. \tag{3.33}$$

The potential is a symmetric function on each type, and so it is described for the site $\boldsymbol{\tau}$ with full angular dependency according to Equation (3.4b), as

$$V(\mathbf{r})|_{r_{\boldsymbol{\tau}}<S_{\boldsymbol{\tau}}} = \sum_h v_{ht}(r) D_{ht}(\mathcal{D}_{\boldsymbol{\tau}}\hat{\mathbf{r}}_t). \tag{3.34}$$

The electrostatic part of the potential is determined by standard methods[36] as,

$$\begin{aligned} v_{ht}(r) = {} & \frac{4\pi e^2}{2\ell_h+1}\int_0^{S_t} dr'\, r'^2\, \frac{r_<^{\ell_h}}{r_>^{\ell_h+1}} n_{ht}(r) \\ & + \left[V_{ht}(S_t) + \frac{4\pi e^2}{2\ell_h+1}\int_0^{S_t} dr'\, r'^2\, \frac{r'^{\ell_h} n_{ht}(r')}{S_t^{\ell_h+1}} \right] \left(\frac{r}{S_t}\right)^{\ell_h} \end{aligned} \tag{3.35}$$

As for the interstitial, the exchange-correlation potential must be calculated from the density directly on a real-space grid, for the muffin-tins expressed in spherical coordinates. The resulting potential is then projected from the angular grid onto the harmonic functions, so that

$$v_{ht}^{XC}(r) = \int d\mathbf{r}\, V^{XC}(\mathbf{r}) D_{ht}(\hat{\mathbf{r}}). \tag{3.36}$$

Combining these with the definition of the basis functions in the muffin-tin we have,

$$\begin{aligned} \mathcal{H}_{ij}(\mathbf{k}) = \langle\phi_i|\mathcal{H}|\phi_j\rangle = {} & \sum_{\boldsymbol{\tau}} \sum_{\ell,m} \mathrm{S}^{\dagger}_{\ell m;\ell_i m_i}(\kappa_i, \boldsymbol{\tau}-\boldsymbol{\tau}_i, \mathbf{k}) \\ \times \Big(& \sum_{\ell' m'} \sum_h \Omega^T_{t\ell}(e_i,\kappa_i) \langle \mathrm{U}^T_{t\ell}(e_i,r)|H_0+v_{ht}|\mathrm{U}_{t\ell'}(e_j,r)\rangle \Omega_{t\ell'}(e_j,\kappa_j) \\ & \langle \ell m|D_{ht}|\ell' m'\rangle \mathrm{S}_{\ell' m';\ell_j m_j}(\kappa_j, \boldsymbol{\tau}-\boldsymbol{\tau}_j, \mathbf{k}) \Big), \end{aligned} \tag{3.37}$$

where summations harmonics are to be taken for components with $\ell_h > 0$, since those are the spherical terms already included in H_0. Here we can clearly see the benefit of making a one-centre expansion of the basis functions. There is only summation over a single $\boldsymbol{\tau}$ index, and the term on the middle line only

has integrals centred on the type t; the information of the off-site contributions to the matrix element is accounted for by the structure functions.

The radial integrals of Equation (3.37) of the form $\langle U_i(r)|H|U_j(r)\rangle$ have contributions of the forms $\langle\phi_i(r)|H|\phi_j(r)\rangle$, $\langle\phi_i(r)|H|\dot{\phi}_j(r)\rangle$ and $\langle\dot{\phi}_i(r)|H|\dot{\phi}_j(r)\rangle$. Since we are using the same basis as is used in the atomic sphere approximation, these matrix elements of H_0 are given by the expressions[57],

$$\langle\phi_{t;\ell_i}(e_i,r)|H_0|\phi_{t;\ell_j}(e_j,r)\rangle = E_t^{ij}\langle\phi_{t;\ell_i}(e_i,r)|\phi_{t;\ell_j}(e_j,r)\rangle \tag{3.38a}$$

$$\begin{aligned}\langle\dot{\phi}_{t;\ell_i}(e_i,r)|H_0|\phi_{t;\ell_j}(e_j,r)\rangle &= E_t^{ij}\langle\dot{\phi}_{t;\ell_i}(e_i,r)|\phi_{t;\ell_j}(e_j,r)\rangle \\ &\quad + \frac{1}{2}\langle\phi_{t;\ell_i}(e_i,r)|\phi_{t;\ell_j}(e_j,r)\rangle\end{aligned} \tag{3.38b}$$

$$\begin{aligned}\langle\dot{\phi}_{t;\ell_i}(e_i,r)|H_0|\dot{\phi}_{t;\ell_j}(e_j,r)\rangle &= E_t^{ij}\langle\dot{\phi}_{t;\ell_i}(e_i,r)|\dot{\phi}_{t;\ell_j}(e_j,r)\rangle \\ +\frac{1}{2}\big(\langle\dot{\phi}_{t;\ell_i}(e_i,r)|\phi_{t;\ell_j}(e_j,r)\rangle &+ \langle\dot{\phi}_{t;\ell_i}(e_j,r)|\phi_{t;\ell_j}(e_i,r)\rangle\big),\end{aligned} \tag{3.38c}$$

where $E_t^{ij} = \frac{1}{2}(E_{t;\ell_i} + E_{t;\ell_j})$ and the last equation has a similar averaging over different energy sets in the ϕ–$\dot{\phi}$ cross terms.

The simple closed forms for these expressions for the contributions from kinetic energy and the spherical part of the potential follow from our choice of basis functions as linear combinations of solutions to the Schrödinger equation for the spherical potential. The remaining integrals for the higher harmonic components, as well as the overlap integrals themselves are performed numerically.

3.4.2 Density

The full electron density inside the muffin-tins is expanded in harmonic functions for each type as shown in Section 3.1,

$$n_t(\mathbf{r}) = \sum_h n_{ht}(r)D_{ht}(\hat{\mathbf{r}}), \tag{3.39}$$

where the site-harmonic-projected density is obtained from the basis functions and the harmonic density coefficients, M_{ht},

$$n_{ht}(r) = \sum_{e\ell}\sum_{e'\ell'} U_{t\ell'}(e',r)M_{ht}(e,\ell;e',\ell')U^T_{t\ell}(e,r). \tag{3.40}$$

These are calculated from a set of intermediate density coefficients, $\mathcal{M}_t$, that hold the m-projected information about the density

$$M_{ht}(e,\ell;e',\ell') = \frac{2\ell_h+1}{4\pi}\sum_{m,m',m_h}\alpha^*(m_h)\mathcal{G}(\ell,m;\ell',m';\ell_h,m_h)\mathcal{M}_t(e,\ell,m;e',\ell',m'). \tag{3.41}$$

The quantities, $\mathcal{M}_t$, can be calculated from the density matrix and the structure functions, scaled by the Ω-matrices and through integration over the Brillouin zone (the $\mathbf{k}$ sums). For each type there is a summation over the $N_{\boldsymbol{\tau}}(t)$ sites of that type, which give rise to the normalisation factor $1/N_{\boldsymbol{\tau}}(t)$.

$$\mathcal{M}_t(e,\ell,m;e',\ell',m') = \frac{1}{N_{\boldsymbol{\tau}}(t)}\sum_{\boldsymbol{\tau}\in t}\sum_{\mathbf{k}}\sum_{i,j}\delta(e,e_i)\tilde{\mathrm{S}}_{\ell m;\ell_i m_i}(e;\kappa_i;\boldsymbol{\tau}-\boldsymbol{\tau}_i;\mathbf{k}) \times \rho_{ij}(\mathbf{k})\tilde{\mathrm{S}}^{\dagger}_{\ell' m';\ell_j m_j}(e';\kappa_j;\boldsymbol{\tau}-\boldsymbol{\tau}_j;\mathbf{k})\delta(e',e_j), \tag{3.42}$$

with the density matrix calculated from a sum over eigenvectors,

$$\rho_{ij}(\mathbf{k}) = \sum_v w_{v,\mathbf{k}}\mathcal{A}_i(v,\mathbf{k})\mathcal{A}^{\dagger}_j(v,\mathbf{k}) \tag{3.43}$$

and the scaled structure constants,

$$\tilde{\mathrm{S}}_{\ell m;\ell_i m_i}(e;\kappa_i;\boldsymbol{\tau}-\boldsymbol{\tau}_i;\mathbf{k}) = \Omega_{t\ell}(e,\kappa_i)\mathrm{S}_{\ell m;\ell_i m_i}(\kappa_i;\boldsymbol{\tau}-\boldsymbol{\tau}_i;\mathbf{k}) \tag{3.44}$$

with i, j being basis function indices. The factor $w_{v,\mathbf{k}}$ is the weight of each eigenvector calculated according to the choice of method for the Brillouin zone integration.

From the matrix $\mathcal{M}_t$ we can also calculate the ℓ-projected average occupancies, $Q_{t,\ell}$, and the orbital moments, $O_{t,\ell}$, resolved per type and ℓ quantum number and, optionally, also in energy sets by taking traces over the m indices

and scaling by the overlap matrix elements,

$$Q_{t,\ell} = \sum_{e,e'} Q_{t,\ell}(e,e') \tag{3.45a}$$

$$\begin{aligned} Q_{t,\ell}(e,e') = \sum_{m=-\ell}^{\ell} & \delta(\ell,\ell')\delta(m,m')\mathcal{M}_t(e,\ell,m;e',\ell',m') \\ & \times \langle U_{t,\ell}(e,r)|U_{t,\ell'}(e',r)\rangle \end{aligned} \tag{3.45b}$$

$$O_{t,\ell} = \sum_{e,e'} O_{t,\ell}(e,e') \tag{3.45c}$$

$$\begin{aligned} O_{t,\ell}(e,e') = \sum_{m=-\ell}^{\ell} & \delta(\ell,\ell')\delta(m,m')\mathcal{M}_t(e,\ell,m;e',\ell',m') \cdot m \\ & \times \langle U_{t,\ell}(e,r)|U_{t,\ell'}(e',r)\rangle. \end{aligned} \tag{3.45d}$$

It is important to note that the energy set resolved quantities only make physical sense if the energy sets are well separated in energy and hybridise very little, that is to say, the off-diagonal components of $Q_{t,\ell}(e,e')$ are small. If this is not the case, the charge density in equation (3.40) is still perfectly fine, but projected partial occupancies may be completely unphysical, with, for example, very large partial occupancies in one energy set and almost equally large but negative occupancies in another. However, in the typical use of different energy sets, with each energy set describing bands derived from different atomic principal quantum numbers, the energies are well separated and such issues do not arise. In this case we may safely interpret the diagonal elements of $Q_{t,\ell}(e,e')$ as valence and semi-core occupancies.

3.5 The total energy

As seen in Chapter 2 the total energy is the sum of the kinetic and potential energies of the single particle part of the problem plus the exchange correlation energy. If we evaluate these for both the core and valence states, and also include the interaction between the nuclei from Equation (2.5), we have,

$$E = T_S^{val} + T_S^{core} + E^C + E^{XC} + E^{NN}. \tag{3.46}$$

The electrostatic and exchange-correlation contributions are readily calculated by their definitions from quantities available at convergence of the SCF cycle. The kinetic energy however is not, since in an actual calculation it is impractical to explicitly construct the Kohn-Sham orbitals and differentiate them, so instead we do the following. If we multiply the Kohn-Sham equations from the left by $\langle \psi_i(\mathbf{r})|$, integrate and sum over the occupied states we

obtain

$$\sum_i^N \langle \psi_i(\mathbf{r})| \frac{\nabla^2}{2} + V^{eff}(\mathbf{r}) |\psi_i(\mathbf{r})\rangle = \sum_i^N \epsilon_i \langle \psi_i(\mathbf{r})|\psi_i(\mathbf{r})\rangle. \tag{3.47}$$

From this the kinetic energy is seen to be

$$T_S^{val} = \sum_i^N \langle \psi_i(\mathbf{r})| \frac{\nabla^2}{2} |\psi_i(\mathbf{r})\rangle = \int_{-\infty}^{E_F} d\epsilon\, \epsilon - \int d\mathbf{r}\, V^{eff}(\mathbf{r})\rho(\mathbf{r}), \tag{3.48}$$

and similarly for the core states, for which the integral is a discrete sum over the occupied states.

The interaction between nuclei is accounted for in the Madelung term which can be expressed in terms of the nuclear charge and the spherical part of the external Coulomb potential at the muffin-tin boundary,

$$E^{NN} = -\frac{1}{2} \sum_t \sum_{\boldsymbol{\tau} \in t} Z_t V_0^C(S_t). \tag{3.49}$$

The exchange-correlation energy must be calculated over both the interstitial and the muffin-tins on a real space mesh. The energy density in the muffin-tins is then expanded, just as the potential, in harmonic functions,

$$\epsilon_{ht}^{XC}(r) = \int d\mathbf{r}\, \epsilon^{XC}(\mathbf{r}) D_{ht}(\hat{\mathbf{r}}), \tag{3.50}$$

and is then multiplied by the corresponding density, integrated and summed over harmonic functions,

$$E^{XC} = \int d\mathbf{r}\, n(\mathbf{r}) \epsilon^{XC}(\mathbf{r}) = \sum_{\boldsymbol{\tau} \in t} \sum_{th} \int d\mathbf{r}\, \epsilon_{ht}^{XC}(r) n_{ht}(r). \tag{3.51}$$

Using these and previous results the total energy is,

$$\begin{aligned} E = \int_{-\infty}^{E_F} d\epsilon\, \epsilon + \sum_{i \in occ} \epsilon_i^{core} + \int d\mathbf{r}\, n(\mathbf{r}) \left(\frac{1}{2} V^C(\mathbf{r}) - V^{eff}(\mathbf{r}) \right) \\ + \int d\mathbf{r}\, n(\mathbf{r}) \epsilon^{XC}(\mathbf{r}) + \frac{1}{2} \sum_t \sum_{\boldsymbol{\tau} \in t} Z_t V_0^C(S_t), \end{aligned} \tag{3.52}$$

with V^C being the total electrostatic (Coulomb) potential.

3.5.1 Constraints and the kinetic energy

We may wish to introduce some additional potential by hand in the Kohn-Sham equations, $\tilde{V}_i$ (such constraints are often orbital dependent, hence the

index i), such as the Lagrangian multiplier associated with some constraint you wish to put on your solutions. In such cases one must correct the kinetic energy by adding

$$T^{corr} = -\sum_i \langle \psi_i | \tilde{V}_i | \psi_i \rangle \tag{3.53}$$

to the right hand side of equation (3.48).

A simple example is that of fixing the magnetic moment of the unit cell. We can do this by adding a constraining potential to each spin channel,

$$\pm V^{fix} \propto \mu^{fix} - \mu^{SCF}. \tag{3.54}$$

The plus and minus apply to the up and down spin channels, respectively, and the constraining potential is taken to be proportional to the deviation of the moment of the SCF cycle from the desired value, μ^{fix}. The correction in equation (3.53) for this case becomes

$$T^{corr} = -\int_{V_{cell}} (V^{fix}\rho^{\uparrow}(\mathbf{r}) - V^{fix}\rho^{\downarrow}(\mathbf{r}))\, d\mathbf{r} = -V^{fix}\mu^{SCF}. \tag{3.55}$$

3.6 Brillouin zone integration

When using the band structure method for solids the wavefunction is written in the Bloch form (2.2), and all expectation values and similar integrals needs to be evaluated by integration of all occupied bands over the Brillouin zone. If we let i label the band and write, $f_i(\mathbf{k})$, for the quantity to be integrated, we have

$$I = \sum_i \int_{BZ} d\mathbf{k}\, w(E_i(\mathbf{k})) f_i(\mathbf{k}), \tag{3.56}$$

where w is the occupation number. The integration is done on a discrete mesh which can be constructed in several ways[21, 51] and we will briefly describe two approaches to evaluating (3.56) that are particularly popular, smearing type methods and the tetrahedron method.

3.6.1 Smearing type methods

In the smearing type methods the integral (3.56) is rewritten as,

$$I = \int_{-\infty}^{\infty} S(\epsilon - E_F) F(\epsilon)\, d\epsilon \tag{3.57}$$

where S is some smooth approximation to the step function, E_F is the Fermi energy, and

$$F(\epsilon) = \int_{BZ} f(\mathbf{k})\delta(\epsilon - E(\mathbf{k}))\, d\mathbf{k}.$$

This gives a particularly simple evaluation of the integral since once we have chosen an approximation to the step function, all we need to do to evaluate (3.57) is to order all eigenvalues for all k-points on our mesh by size and sum up to the highest one that is non-zero.

The most common approximation for the step function is a series of Hermite's functions[50],

$$S_0(x) = \frac{1}{2}(1 - \mathrm{erfc}(x)) \tag{3.58}$$

$$S_N(x) = S_0(x) + \sum_{n=1}^{N} A_n H_{2n-1}(x) e^{-x^2}, \tag{3.59}$$

where, $\mathrm{erfc}(x) = \int_{-\infty}^{x} dt\, e^{-t^2}$, is the error function and $x = \frac{E-E_F}{\sigma}$. This expression then contains two parameters to be chosen, the integer N to use for the truncation of the series (3.59), and the smearing parameter, σ. Using a larger smearing will improve the convergence of the SCF procedure since small changes in the Fermi level will be lost in the smearing and stability to small occupation changes is therefore enhanced. However, if the quantity we are interested in depends on such small changes of occupation all such information has been lost and the result is not accurate enough.

3.6.2 The tetrahedron method

The tetrahedron method evaluates the integral by using the k-points to divide the space into tetrahedra. After obtaining a value of the band for the k-point in each corner the band is then linearly interpolated through the tetrahedron[38, 46]. This will give give the filling of this tetrahedron[5], and from that number, the occupations of Equation (3.56) for each of the k-points can be calculated. A quadratic correction formula that drastically improves the convergence has also been constructed by Blöchl *et al*.[11] Unlike the smearing type of methods the tetrahedron method has no adjustable parameter, but instead derives the weights directly from the linear approximation of the band dispersion.

For future reference we illustrate how a cube can be partitioned into tetrahedra of equal volume in Figure 3.2. The general scheme followed is as follows.

1. Select one corner of the cube, label it 1, and draw the body diagonal from this corner.

[5] That is, how large portion of the tetrahedron that is within the Fermi surface.

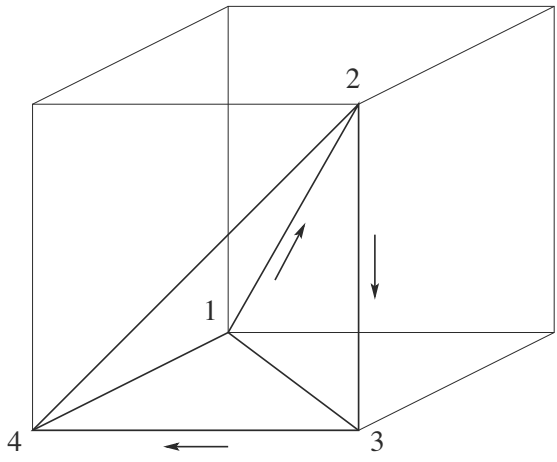

Figure 3.2: Illustration of the steps in partitioning of a cube into equal tetrahedra.

2. Following the body diagonal, label the next corner 2.
3. Follow either of the three possible edges to the next corner. Label this 3.
4. Continue along one of the next two possible edges and label the next corner 4.
5. Draw the remainder of the lines to connect these four corners. This is one of the tetrahedra.
6. Repeat the procedure in all possible different ways. There will be 6 different ways, since along each way we get first a choice of three and then a choice of two.

All tetrahedra generated in this way will share the initial body diagonal as one of its sides and looking at Figure 3.2 we can easily see that a partitioning generated by the above scheme leaves us with a construction that does not have the symmetry of the original cube. The use of the tetrahedron method has broken the cubic symmetry in this case.

3.6.3 Paper VII. Adaptive Gaussian smearing

The tetrahedron method has the great benefit of not needing any adjustable parameters, which has made it popular to determine very sensitive quantities. One such property is the magnetocrystalline anisotropy energy (MAE), the difference in energy between different magnetisation directions, which in cubic materials can be on the order of 0.1μeV[13]. Unfortunately, the breaking of the cubic symmetry as described above means that directions that in a cubic lattice should be equivalent no longer are. This leads to inconsistent results of the MAE, giving different energy differences depending on which choice of supposedly equivalent axis we choose.

The adaptive Gaussian smearing (AGS) scheme was developed in an attempt to circumvent this problem. Smearing types of methods do not break the symmetry, since the it uses each k-point individually without considering its surrounding k-points. Thus, if we can find a way to eliminate the smearing parameter, these schemes should be better for calculating the MAE in sensitive materials. In Paper VII we present a way to eliminate the smearing parameter by adaptively decreasing it depending on the density of the k-point mesh. We suggest using the formula

$$\sigma = \frac{3\sqrt{2W}}{4\pi m^*} \left(\frac{V_{BZ}}{n_k} \right)^{1/3} \tag{3.60}$$

where W is the width of the valence band, n_k is the number of k-points, V_{BZ} is the Brillouin zone volume and m^* is an effective mass parameter that needs to be given. This still leaves one parameter to be set *ad hoc*, the effective mass parameter, but we demonstrate that for any value of m^* in a physically reasonable range the calculation will converge to the same answer, independent of this choice.

When tested, the AGS scheme did not yield the convergence properties of the MAE that was anticipated, we did not manage to converge total energy differences to the μeV level. Nevertheless the scheme seems robust on the energy scales practitioners in the *ab initio* solid state field usually work with, and we think that the AGS scheme will be found useful in the future.

3.7 Technical remarks on the FP-LMTO method

3.7.1 The quality of the basis set

A fundamental problem in the FP-LMTO method is to judge the quality of the basis set. We know that the individual basis functions are rather close to the true solution—if we had employed the atomic sphere approximation we would even have been content with a single one of them—but it is not obvious how to proceed to improve on this choice by adding more functions of the same shape. Nor is there any obvious general criterion for how to determine whether the basis is a good one. We will now outline one possible such criterion that has been found to be useful, along with a suggested procedure to arrive at a good basis.

We choose to take as a measure of the quality of the basis how dependent the final solution is on the choice of muffin-tin radius R_{MT}. That our total energy is independent of R_{MT} can be crucial when we wish to determine structural stabilities between structures or compounds with different packing ratios. In such cases, the geometry forces us to choose different muffin-tin radii for the different calculations, and a strong dependence of the final result on R_{MT} may cause large errors. As an example we may look at the smallest

possible fraction of the interstitial volume to the total volume of the cell for the cubic close packed structure (fcc) and the much more open zinkblende structure. The smallest possible value of the interstitial volume[6] for the fcc is 26%, while it is 66% for the zinkblende structure.

Traditionally, there are two ways of constructing a basis set for the FP-LMTO method. The first is based on a tail setup (number of tails and κ^2 values) as described in the original main reference of the method[76]. This setup, referred to as "default" since it is generated as default by the program, is based on calculations for the actinide metals and consists of a triple-κ basis for the valence s and p states and a double-κ basis for the remainder of the states, be they semicore or valence states. There are two κ^2 values common to all basis functions, 0.3 Ry and -2.3 Ry, and the additional tail of the valence s and p states has $\kappa^2 = -0.6$ Ry. In this approach every ℓ-shell has basis functions with tails that span the entire range of the physical energies involved. The individual tails are typically not seen as carrying physical content, but it is sometimes convenient to set the highest tail equal to the average kinetic energy of the interstitial. The proper separation of the semicore and the valence states is imposed by fixing the logarithmic derivative at the muffin-tin sphere of the valence states to be the same as that of the semicore states (but having one more node in the wavefunction, since they describe different principal quantum numbers).

The second approach to basis set construction has been gradually developed in Uppsala and will therefore be referred to as the "Uppsala" setup. This associates more physical content with the basis, and so a double-κ basis will use four different tail energies, two for the valence and two for the semicore. These four tail energies are all chosen to be negative, by roughly the following scheme.

1. Set the highest tail energy, $\kappa^2 = -0.1$ Ry.
2. Set the lowest tail energy, $\kappa^2 \approx$ the difference between the lowest semicore eigenvalue and the Fermi level.
3. Space the remaining tails evenly between the first two.
4. Attach the two lower to the semicore states and the two higher to the valence states.

The separation between semicore and valence states is enforced by choosing E_ν to be the band centre for the semicore states, and then minimise the energy only with respect to the E_ν for the valence states. Typically this basis set will yield higher total energies than the default setup, and so can be seen as less good. In practice, however, little difference is found when calculating energy differences and physical properties and one often finds a faster convergence of the ground state calculations than with the default setup. It is surmised that this property and the systematically higher total energies is due to the harder constraint put on the semicore states which has a large contribution to the

[6]The value for which we have the muffin-tin spheres *almost* touching.

total energy but usually do not take active part in physical properties that are calculated.

We now proceed to evaluate these two approaches in terms of the total energy and its dependency of the muffin-tin radius. We show here an example where a heavy element, fcc lead, has been calculated without spin-orbit interaction[7], and the total energies, offset by an arbitrary constant, are shown in Figure 3.3. The Default setup is shown (dashed) and it has also been supplemented with a version where the top tail has been replaced with a tail with $\kappa^2 = \bar{T}_{Int}$, the average kinetic energy over the interstitial (dotted). The result of the Uppsala setup is shown as a dashed-dotted line. We can see that using the average kinetic energy as one tail improves the result, since the energy is lowered and the variation from the muffin-tin dependency is smaller. The Uppsala setup has a higher total energy for almost the whole range of muffin-tin radii, but is somewhat better for small radii. Both perform quite poorly seen over the whole range of values but we can note that if we restrict ourselves to the range from fcc to zinkblende interstitial volume fractions ($\sim 0.26 - 0.66$) the variation is on the order ~ 5 mRy, which is quite acceptable.

As we see, both basis sets seem to have their strong points in this comparison, and it seems plausible that combining some ideas in the two setups might be worthwile. We do this by choosing the lower tails from the Uppsala setup and from the Default setup we take the one positive (”interstitial average”) tail together with the means to separate semicore and valence states by fixing the logarithmic derivative of the valence states. As is seen from Figure 3.3 the result is a drastic improvement over the two other basis sets. Also included is a calculation using the average interstitial energy as the highest tail, which is virtually indistinguishable from the fixed tail since the average interstitial energy happened to end up very close to the chosen fixed energy. We get the lowest total energy and the maximum deviation over the whole range of radii is only ~ 2.5 mRy.

If we study actual physical properties we can see the effect of the improved basis set clearly. In Table 3.1 we show what can be achieved for the equation of state of lead if a suitably good basis is chosen. With the Default basis we obtain a good equilibrium volume and a reasonable bulk modulus, but with the improved basis set even the derivative of the bulk modulus with respect to volume is in agreement with experiment. In particular, the AM05 functional performs very well in this case.

3.7.2 Performance aspects of the FP-LMTO method

When performing electronic structure calculations it is good to have an understanding of computational performance of the code. In the following we out-

[7]The spin-orbit part of the Hamiltonian is only evaluated over the muffin-tins, and so the Hamiltonian itself is depends on the muffin-tin radius and we could not tell which variation comes from the basis and which come from the spin-orbit term.

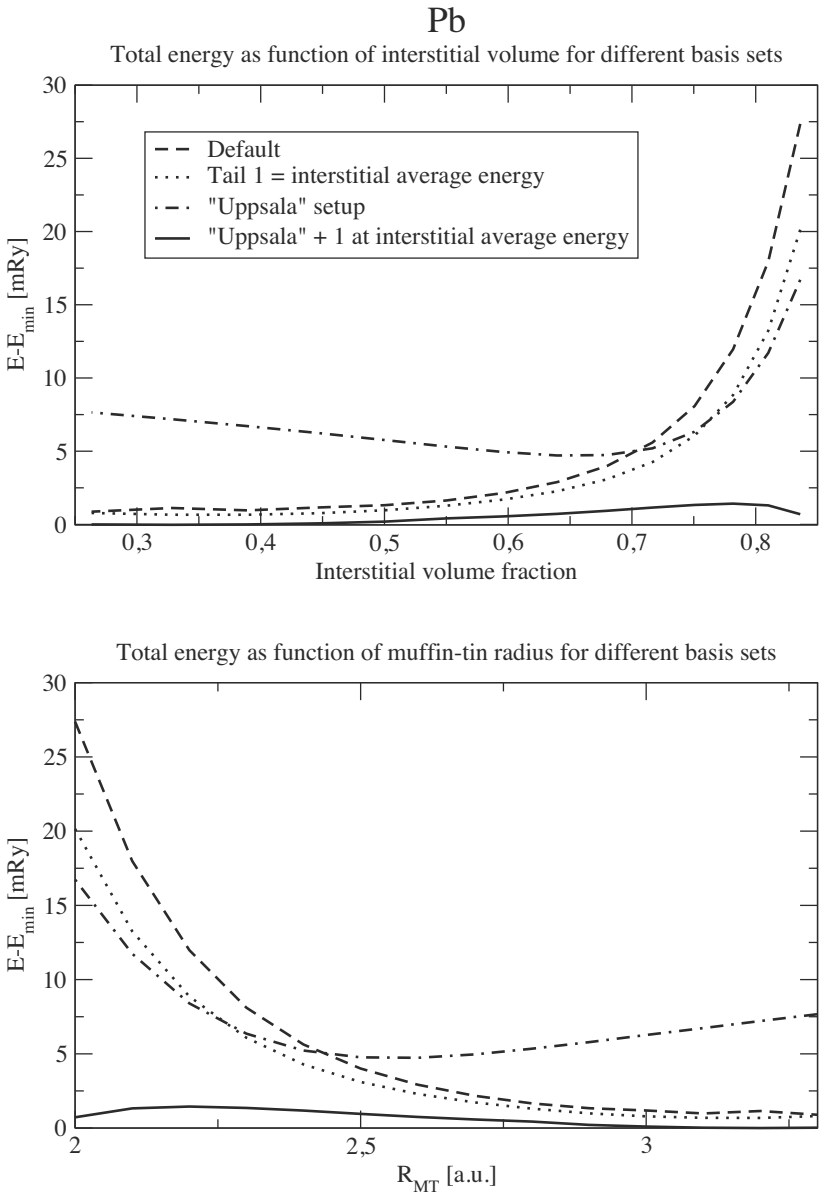

Figure 3.3: The total energy as function of the interstitial volume fraction (upper panel) and the muffin-tin radius (lower panel) for a ground state calculation, excluding spin-orbit coupling, of fcc Pb at the experimental lattice constant. The result is drastically different depending on the choice of basis set. See text for explanation of the terms in the legends.

Table 3.1: *Comparison of the equilibrium volume, V_0 and the bulk modulus, B_0 and derivative of the bulk modulus, B_0', for the Default basis set and the improved basis set described above (labelled New). Calculations were made for three different exchange-correlation functionals, LDA (von Barth-Hedin[74]), PBE96[53] and AM05[7]. Spin-orbit coupling is included in these calculations.*

		V_0 (Å^3)	B_0 (GPa)	B_0'
	Experiment[43]	30.31	40.5	5.74
New	LDA	29.3	49.6	4.91
	PBE96	32.4	37.2	4.40
	AM05	30.5	41.5	5.39
Uppsala	LDA	29.7	47.5	4.85
	PBE96	32.9	35.3	4.67
	AM05	31.0	39.9	4.87
Default	LDA	29.2	52.3	8.50
	PBE96	32.4	37.5	3.07
	AM05	30.4	37.7	11.7

line some details of the implementation of the full-potential LMTO method in the software package RSPt[1].

3.7.2.1 Brief tour of the numerics

The RSPt code relies for its performance heavily on the external libraries BLAS, LAPACK and FFTW for linear algebra and Fourier transforms. In particular, calls to BLAS functions are extensively used to take care of the innermost part of nested loops[8]. This means that for high performance it is essential to link with highly optimised versions of BLAS and LAPACK, but there is not a very large improvement by turning on the highest optimisation flags in the compiler.

The process of calculation in a normal electronic SCF step is sketched in Figure 3.4. The division in blocks is the same as in the actual computation, and by looking for the words `eigen`, `conden` and `conpot` in the `out` file you will find timings for the different parts. The different blocks do the following:

`eigen` – Sets up the Hamiltonian and overlap matrices and solves the generalised eigenvalue problem for all vectors on the k-point mesh. Finds the Fermi level and computes the eigenvalue sum.

[8]Element-wise multiplication and addition of two double precision vectors are for example taken care of with a call to the BLAS scalar multiplication function `ddot`.

conden – Computes the density, $n(\mathbf{r})$, throughout the unit cell from the eigenvectors, eigenvalues and basis functions by integration over the occupied part of the Brillouin zone.

conpot – Computes the potential and then calculates the total energy.

There are also initialisation blocks before these three, doing various preliminary calculations that are not performance critical (setting up lattices, preparing the calculation of the muffin-tin matrix elements, initialising the FFT's etc.) and we therefore lump them together as simply "Initialisations".

A few things are to be noted here.

- The FP-LMTO method is based on a set of rather complex basis functions. The calculation of the matrix elements therefore takes significant time.
- The computations of all quantities are in principle done twice — once for the muffin-tins and once for the interstitial. These two parts may behave rather differently performance-wise, for example as soon as interstitial quantities are to be handled there are Fourier transforms involved, whereas the muffin-tins instead always have summations over structure functions. The former do not scale directly with the number of basis functions, but the latter do. We will see the effect of this later.
- The blocks `eigen` and `conden` are the only parts that depend on the k-space mesh.

3.7.2.2 Analysis of performance

We study two examples that stress the code in different ways.

1. An fcc Ce $3 \times 3 \times 3$ supercell (27 atoms). The Fourier mesh was $60 \times 60 \times 60$ and there were 3 k-points in the irreducible Brillouin zone (IBZ). The default basis with $5s$-states in the core was used (intermediate, fairly typical size of basis).
2. A simple fcc Ni cell (one atom) with inversion as the only symmetry operation. The Fourier mesh was $20 \times 20 \times 20$, and number of k-points in the IBZ was 27652. The default basis with $3s$ and $3p$ states in the core was used (rather small basis).

In the first case the problems come from the large cell, which gives us many basis functions and the fact that we need a large Fourier mesh to get sufficient resolution in real space. In the second case the only problem is the large set of k-points. The calculations are in both cases the first electronic iteration of a simple ground state run. The number of k-points for the Ni calculation has been chosen so that the total runtime is very similar in the two cases, and so allows for a very direct comparison of how the run time is distributed between different tasks within the code both for a large and a small cell. The tests were performed on an Intel Harpertown 2.66GHz CPU.

If we look at the first section of the breakdown of timings (Table 3.2) we see that the time spent in the different parts of the code does not seem to change. The main difference is that conpot, the potential calculation, is much larger in

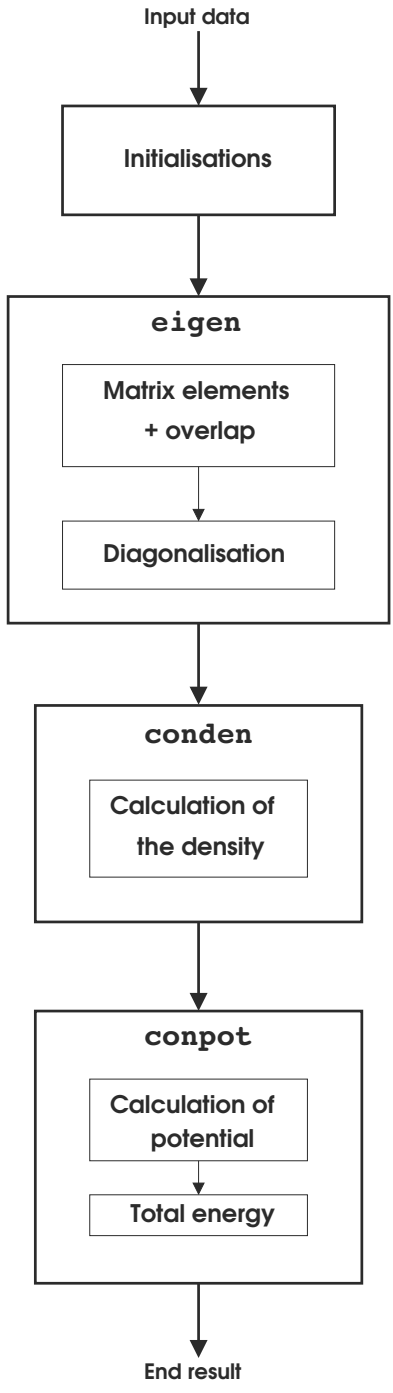

Figure 3.4: Sketch of the principal layout of the RSPt band structure program.

Table 3.2: *Breakdown of the significant timings for two RSPt runs for one Ce supercell (3 k-points) and one fcc Ni cell (27652 k-points). The timings are broken down in two different ways, after block of code and depending on the numerical task performed. Note that the different calculations in the Tasks section may overlap, so the total is not the sum of all numbers in the column. All times are in seconds.*

	Numerical Computation	Ce supercell	fcc Ni
Blocks	`eigen`	985	996
	`conden`	214	270
	`conpot`	13	< 1
Tasks	Hamiltonian + overlap	652	913
	Matrix diagonalisation	285	31
	Fourier transforms	145	687
	Total	1228	1269

the supercell, but still very small. The reason for the large difference is that the potential is not k-dependent and so the calculation is very fast in the small Ni cell.

If we turn to the second section in the table we see that the time is spent doing slightly different things in the two cases. Note that in this section the different timings overlap, since the Hamiltonian+overlap calculation contains Fourier transforms. In the supercell the larger basis gives us a matrix that takes longer to diagonalise. This takes a barely noticeable time for the small cell. In the small cell instead nearly all time is spent setting up the matrix elements, and we see that a large amount of this time is spent doing Fourier transforms. For a large cell the muffin-tin part is a larger portion of the total time. The part that mainly grows in the muffin-tin part is summations over structure functions, which are not present for the interstitial potential matrix elements because of the use of the pseudo basis[9]. Thus it seems that the structure function summations scale worse with system size than the FFT's.

In conclusion we can say that for a given size of the k-mesh, the two factors that determine the speed of the calculations are the size of the Fourier mesh and the size of the basis, the first being the more important. For small systems, one should use as small a Fourier mesh as possible and for large systems it is also important to ensure that the basis is not to large. The whole calculation will scale linearly with the number of k-points.

[9]Nevertheless, structure functions enter the interstitial matrix elements in the evaluation of the overlap, and from that the kinetic energy.

4. Self-interaction corrections in band theory

4.1 The self-interaction

When we set up the expressions for the total energy of an N-electron system we had the Hartree term

$$E^H = \frac{1}{2}\int \frac{\rho^N(r)\rho^N(r')}{r-r'}drdr' = \frac{1}{2}\int V^N(r)\rho^N(r)dr \tag{4.1}$$

for the "classical" part of the static Coulomb interaction of a distribution, ρ^N, of N electrons. Written in this form it is easy to spot that this is incorrect. What we sum up is the electrostatic energy of N electrons in the presence of the electrostatic field from the same N electrons. While this would be right for a continuous charge distribution, it is incorrect for a distribution of discrete charges moving in the potential created by all other charges. The appropriate expression is instead

$$\frac{1}{2}\int \frac{\rho^N(r)\rho^{N-1}(r')}{r-r'}drdr' = \frac{1}{2}\int V^{N-1}(r)\rho^N(r)dr, \tag{4.2}$$

where we have the appropriate form of the interaction with each electron moving in the field created by the remaining $N-1$ electrons. To directly correct this error by calculating the appropriate potential V^{N-1} is cumbersome, as it would require you to solve an additional $N-1$ electron system on the side throughout your calculation. Fortunately a neater way automatically presents itself through the Hartree-Fock approximation, and this will then carry over directly to the various approximations to the exchange-correlation energy in DFT.

As we saw earlier in Chapter 2, in Hartree-Fock we have for the electrostatic interaction in addition to the Hartree term the exchange term

$$E^X = \sum_{i,j}\int \frac{\psi_i^*(r_1)\psi_j(r_1)\psi_j^*(r_2)\psi_i(r_2)}{r_1-r_2}dr_1dr_2. \tag{4.3}$$

By re-expanding the charge densities of (4.1) in its wave function components, we can write the Hartree term in the form

$$E^H = \sum_{i,j} \int \frac{\psi_i^*(r_1)\psi_i(r_1)\psi_j^*(r_2)\psi_j(r_2)}{r_1 - r_2} dr_1 dr_2. \tag{4.4}$$

The interaction of a particle with itself is obtained by setting $i = j$ in these two-electron integrals, and we then see that the self-Hartree interaction is exactly cancelled by a self-exchange interaction. Thus in Hartree-Fock the problem automatically goes away. In LDA and other functionals commonly used in the Kohn-Sham scheme, however, the cancellation of the self-Hartree and self-exchange-correlation energies for a single orbital is incomplete,

$$E^H[n_\alpha(\mathbf{r})] + E^{XC}[n_\alpha(\mathbf{r})] \neq 0. \tag{4.5}$$

In solids, this turns out to be a problem mainly for localised states, typically of d and f character, for which the self-interaction is large. This favours solutions to the KS equations which have itinerant d- and f-electrons over the localised solution, and yields a spurious bonding that give completely wrong results for many d- and f-systems such as the elements in the lanthanide series.

4.2 The correction

A few words on the notation in what follows is in order. Quantities associated with the self-interaction of a single-electron state will be denoted by the superscript SI, and quantities that has been corrected for the self-interaction will have the superscript SIC. The approximation for the effective potential and energy functionals will be denoted LDA throughout, but it could equally well be any other approximation such as a GGA or hybrid functional. We also need to introduce a notation in relation to the exchange-correlation functionals. The functionals are typically parametrised in terms of the Wigner-Seitz radius, $r_s = \left(\frac{4\pi n(\mathbf{r})}{3}\right)^{-\frac{1}{3}}$, and the polarisation, $\zeta = \frac{n^\uparrow(\mathbf{r}) - n^\downarrow(\mathbf{r})}{n(\mathbf{r})}$, which is one for a fully polarised density and 0 for a non-polarised one. Following the common notational customs we write,

$$E^{XC}[n^\uparrow(\mathbf{r}), n^\downarrow(\mathbf{r})], \tag{4.6}$$

to denote the spin-polarised functional.

4.2.1 The Perdew-Zunger prescription

Inspired by the orbital-by-orbital cancellation of the self-interaction in Hartree-Fock theory Perdew and Zunger[54] suggested to remedy the

incomplete cancellation of the self interaction by simply prescribing that for each occupied orbital, α, the quantity in Equation (4.5) should vanish. They argued that as each electron state should be considered as being completetly spin polarised, and we get the following correction to the energy functional

$$E^{SIC}[n] = E^{LDA}[n] - \sum_{\alpha} \left(E^{H}[n_\alpha] + E^{XC}[n_\alpha, 0] \right). \tag{4.7}$$

We also get a corresponding correction to the potential for the electron in the state α,

$$V_\alpha^{SIC} = V^{LDA}[n] - (V^{C}[n_\alpha] + V^{XC}[n_\alpha, 0]). \tag{4.8}$$

Note the functional argument 0 that denotes that the state is completely spin-polarised. From this point on we will drop the two arguments and just write, $E^{XC}[n(\mathbf{r})]$ etc., and need to remember that the self-interaction corrected states have $\zeta = 1$.

We now have an orbital-dependent potential which results in the Kohn-Sham-SIC equations,

$$\left(\frac{\nabla^2}{2} + V^{LDA} - (V_\alpha^C + V_\alpha^{XC}) \right) \psi_\alpha = \sum_{\alpha'}^{occ.} \varepsilon_{\alpha,\alpha'} \psi_{\alpha'}, \tag{4.9}$$

where the Lagrange multipliers on the right hand side now form a matrix, and the summation on the right hand side is taken over occupied states. This is to construct solutions which are orthogonal, despite the fact that the eigenfunctions, ψ_α, are solutions to different Hamiltonians since they all see a different potential. There are different ways to tackle the problems that the off-diagonal Lagrange multipliers introduce, and now follows an outline of the unified Hamiltonian method[32, 33, 66]. Another solution is to use a steepest descent method to search for the values of the $\varepsilon_{\alpha,\alpha'}$ matrix that gives energy minimum[64].

In the unified Hamiltonian the aim is to transform Equation (4.9) into a form where the Hamiltonian absorbs the off-diagonal Lagrange multipliers—we effectively move them to the left hand side of the equation, and then solve the resulting problem as usual. This can be done by the following transformation,

$$H_u = \sum_{\alpha}^{occ.} (\mathcal{P}_\alpha H_\alpha^{SIC} \mathcal{P}_\alpha + \mathcal{O} H_\alpha^{SIC} \mathcal{P}_\alpha + \mathcal{P}_\alpha H_\alpha^{SIC} \mathcal{O}) + \mathcal{O} H^{LDA} \mathcal{O}. \tag{4.10}$$

We have introduced H_α^{SIC} for the Hamiltonian of the α orbital and the projection operators $\mathcal{P}_\alpha$ and $\mathcal{O}$ which projects onto the orbital α and the space of non-SIC states, respectively. Specifically,

$$\mathcal{O} = \sum_{\alpha}^{occ.} (\mathbf{1} - \mathcal{P}_\alpha). \tag{4.11}$$

In this work we will neglect the off-diagonal Lagrangian multipliers, thus having states that are not exactly orthogonal, and for this case the transformation (4.10) reduces to the much simpler

$$H'_u = H^{LDA} + \frac{1}{2}\sum_{\alpha}^{occ.}(\Delta H_\alpha^{SIC}\mathcal{P}_\alpha + \mathcal{P}_\alpha \Delta H_\alpha^{SIC}), \tag{4.12}$$

where $\Delta H_\alpha^{SIC} = H_\alpha^{SIC} - H^{LDA}$ is the difference between the SIC and the LDA Hamiltonians for the state α.

To better get a feeling for the consequences of the SIC correction of the Hamiltonian, let us consider ΔH_α^{SIC} more explicitly. H^{SIC} is simply H^{LDA} with an added term $-V_\alpha^{SI}$, so a diagonal matrix element of the Hamiltonian is modified by an amount

$$\begin{aligned} -\Delta\varepsilon^{SIC} &= -\langle\,\psi_\alpha|\,V^{SI}\,|\psi_\alpha\,\rangle = \\ &\int d\mathbf{r}\,\psi_\alpha^*(\mathbf{r})V^{SI}[n_\alpha(\mathbf{r})]\psi_\alpha(\mathbf{r}) = \int d\mathbf{r}\,\left(V^{SI}[n_\alpha(\mathbf{r})]\right)n_\alpha(\mathbf{r}). \end{aligned} \tag{4.13}$$

We will assume that the quantity V^{SI} is positive (the Hartree potential is typically larger than the exchange-correlation potential), so the potential correction will shift the eigenvalue down in energy.

4.2.2 The Lundin-Eriksson prescription

A somewhat different correction scheme was proposed by Lundin and Eriksson[49]. They argued that to get the proper correction one ought not to subtract the energy of the orbital density from the energy of the total density, but instead subtract the orbital density from the total density and evaluate the functional for this quantity. This will make no difference for the Hartree term, but the nonlinear dependency of the exchange-correlation energy on the density will result in a different outcome for that quantity. The expression for the self-interaction corrected energy is then

$$\begin{aligned} E^{LE-SIC} &= E^{LDA}[n(\mathbf{r})] \\ &\quad -\sum_\alpha \left(E^H[n_\alpha(\mathbf{r})] + (E^{XC}[n(\mathbf{r}) - n_\alpha(\mathbf{r})] - E^{XC}[n(\mathbf{r})])\right). \end{aligned} \tag{4.14}$$

The potential correction changes accordingly, and we have the following expression for the SIC eigenvalue shift,

$$\begin{aligned} \Delta\varepsilon_\alpha^{LE-SIC} = \int d\mathbf{r}\,\Big[&V^{LDA}[n^{LDA}(\mathbf{r}) - n_\alpha(\mathbf{r})] \\ &- V^{LDA}[n^{LDA}(\mathbf{r})]\Big]n_\alpha^{SIC}(\mathbf{r}). \end{aligned} \tag{4.15}$$

4.3 The relation to LDA+U

Another popular method for correcting the the Coulomb interaction of LDA is the LDA+U method. The method introduces the quantities U and J, the for the direct and the exchange part of the on-site interaction, and assumes that there exists some means of determining these quantities. Although many practitioners of the method use U as an adjustable parameter, the way to obtain a suitable U parameter was originally the so-called constrained LDA (C-LDA) [26], and seen from this perspective, the LDA+U bears a simple relationship with the LDA+SIC method.

Taking a first and most basic shot at a value for the U parameter is to say that the direct part of on-site Coulomb interaction is equal to the Slater integral $F^0(\alpha,\alpha)$ from standard atomic theory[15]

$$U_\alpha = F^0(\alpha,\alpha). \tag{4.16}$$

This unfortunately gives a value that is much to large since in solids, the value of $F^0(\alpha,\alpha)$ is significantly screened by other electrons. We first give a hand-waving argument for how to obtain U in the SIC scheme. Slater noted that the unscreened parameter $F^0(\alpha,\alpha)$ in Hartree theory is just the spherical average of the (Hartree) self-interaction[59]. By instead using the spherical average of the full LDA self-interaction we get a screening of the Hartree self-interaction by the self-exchange-correlation. This reduces the value of $F^0(\alpha,\alpha)$, not accounting for relaxation of the orbitals and the local environment. We will now show in more detail how the value of $\Delta\varepsilon^{SIC}$ ends up close to the U parameter as calculated from C-LDA.

Invoking Janak's theorem[37], Gunnarsson et al. obtained for an orbital, α, in the correlated subshell

$$U = \frac{\partial \varepsilon_\alpha^{LDA}}{\partial n_\alpha}. \tag{4.17}$$

To evaluate this derivative, the charge density of the correlated subshell is then constrained to contain some number of electrons, different from the LDA result, $n_\alpha^{LDA} + \Delta n_\alpha$, and the shift of the eigenvalue is calculated using a formula from first order perturbation theory

$$\begin{aligned}\Delta\varepsilon^{C-LDA} &= \varepsilon_\alpha^{LDA}[n_\alpha^{LDA} + \Delta n_\alpha] - \varepsilon^{LDA}[n_\alpha^{LDA}] \\ &\approx \int d\mathbf{r}\left(V[n_\alpha^{LDA}(\mathbf{r}) + \Delta n_\alpha] - V[n_\alpha^{LDA}(\mathbf{r})]\right)\left(\phi_\alpha^{LDA}(\mathbf{r})\right)^2. \end{aligned}\tag{4.18}$$

According to Slater's transition state rule[59], the optimal way of evaluate this quantity is by using the values $\Delta n_\alpha = \pm\frac{1}{2}$, as was done in the first LDA+U implementation[6]. However, the results of Gunnarsson et al. in Reference [26] indicate that the slope of $\Delta\varepsilon/\Delta n_\alpha$ is not highly sensitive to the choice of Δn_α. If one instead makes the choice $\Delta n_\alpha = -1$, that is, to calculate the

difference from n^{LDA} to a state with one electron less, the right hand side of equation (4.18) almost coincides with equation (4.15), the shift of the SIC eigenvalue in the Lundin and Eriksson scheme. If the orbital, ϕ_α, in equation (4.18) is allowed to relax from the LDA value in response to the difference in occupation, the content of the two equations will essentially be the same as the result of the fully relaxed C-LDA, since in a fully self-consistent calculation both the local orbitals and the environment is allowed to relax in response to the altered occupation of the α orbitals. We may therefore consider it justified to say that

$$\Delta\varepsilon^{C-LDA} \approx \Delta\varepsilon^{SIC}. \tag{4.19}$$

So the constrained LDA scheme can be seen as a way of obtaining the self-interaction, and conversely, the self-interaction correction provides as a by-product a value of the screened Coulomb interaction (as determined from LDA). This could be put to good use in LDA+U calculation as a way to obtain the U parameter automatically and self-consistently, as our procedure for determining $\Delta\varepsilon^{SIC}$ from a core state can be performed independently from any other calculations involved in a self-consistent scheme.

4.4 Paper I. SIC in the FP-LMTO method

In Paper I the implementation of SIC in the FP-LMTO method is described. This section mainly restates the information of Paper I in a slightly different way, and in some instances more details are given, in particular, some results for atoms using the core state solver are given.

4.4.1 SIC for a core state

Before describing the full implementation of the self-interaction correction for the valence electrons in a crystal it is instructive to see how it can be applied to the simpler case of a core state. Using the LDA effective potential, V^{LDA}, we first get a core wave function, $\phi_\alpha(r)$, of the selected orbital, α (e.g. a d or f state). We then use this to obtain a spherical density for an electron in the α-shell squaring the wave function.

$$n_\alpha(r) = |\phi_\alpha(r)|^2. \tag{4.20}$$

We now determine the contribution to the total potential that comes from the self-interaction of the α-shell electrons as in equation (4.8) above.

$$V_\alpha^{SI}(r) = V_C[n_\alpha(r)] + V_{XC}[n_\alpha(r), 0] \tag{4.21}$$

We then subtract the self-interaction from the LDA potential to get a corrected potential, determine new α-shell wave functions and reiterate until $V^{SI}(r)$ is converged. The procedure is illustrated in Figure 4.1.

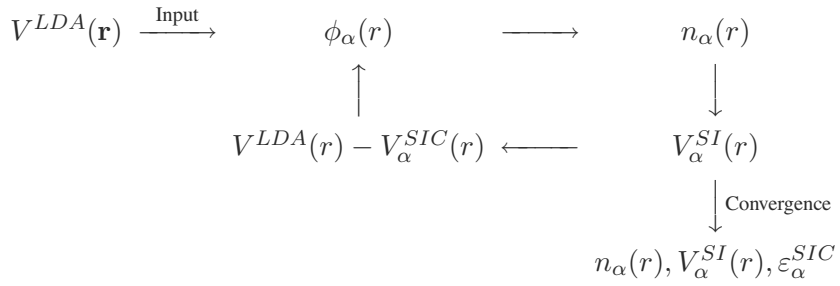

Figure 4.1: The self-consistent cycle determining the SIC potential, $V^{SIC}(r)$, the SIC eigenvalue, ε^{SIC}, for a core eigenstate.

Once we have determined the SI corrected density, $n_\alpha(r)$, it can be added to the total density and the eigenvalue is added to the core eigenvalue sum as usual. We must also evaluate the SIC contribution to the total energy from equation (4.7) for the density $n_\alpha(r)$, and, since we modify the Hamiltonian by hand with an additional potential for part of the density, we also need to add a correction to the kinetic energy as shown in equation (3.53). In the present case the kinetic energy correction is simply the shift of the energy eigenvalue,

$$T^{corr} = \Delta\varepsilon_\alpha^{SIC} = \int_0^{S_{co}} dr\, n_\alpha^{SIC}(r)\, V_\alpha^{SIC}(r). \tag{4.22}$$

4.4.2 SIC for valence states

There are many ways to apply the self-interaction correction to the valence states of a solid. The present scheme is based on the idea that the correction is to be used to describe localised states in the solid when LDA fails to do so correctly. It is therefore useful in the following to think of the SIC state as describing electrons sitting in atomic-like states on a single lattice site. These states form, in general, an open atomic shell which in the crystalline environment will have a non-spherical charge density and may hybridise to some extent with other states in the solid. It is therefore insufficient to treat these states as core states, which by construction are always spherical and cannot hybridise with any other states. The LMTO machinery is particularly well suited for special treatment of localised states, since the basis functions are local solutions to the Schrödinger equation for each site.

Since we will be describing localised, atomic-like states, our basis for the calculation of the self-interaction of a valence state is the procedure described

above for a core state. We use the procedure illustrated in Figure 4.1 for a core state corresponding to the valence shell we intend to correct. This will give us the self-interaction part of the potential, V_α^{SI}, an eigenvalue ε_α^{SIC} and the shift of the LDA eigenvalue, $\Delta\varepsilon_\alpha^{SIC}$. This way of defining the SIC state is very closely related to the previous implementation known as *local SIC*[48].

The procedure for a SIC calculation is then implemented essentially in three parts;

1. Modification of the Hamiltonian.
2. Optionally modify of the LMTO basis.
3. Projection of the SIC valence density and evaluation of the SIC functional.

4.4.3 Modifying the Hamiltonian

To modify the Hamiltonian we must decide on which single-particle states we wish to correct. The choice is made as a some linear combination of m_ℓ and spin quantum numbers for a state centred on some site

$$|\alpha\rangle = \sum_{m_\ell,\sigma} c_{m_\ell,\sigma}|m_\ell,\sigma\rangle, \tag{4.23}$$

where the coefficients, $c_{m_\ell,\sigma}$ need to be chosen by physical intuition. We will mostly chose crystal field states, such as the T_{2g} and E_g states for d-electrons, in ways that conserve the symmetry of the lattice. The problem of choosing appropriate single-particle states will be discussed in more detail later.

We now get the SIC Hamiltonian matrix elements by constructing projectors for all our chosen occupied states, $|\alpha\rangle\langle\alpha|$, and add these to the LDA Hamiltonian

$$H_{ij}^{SIC} = \langle i|H^{LDA}|j\rangle + \sum_{\{\alpha\in occ.\}} \langle i\,|\alpha\rangle\langle\alpha|\,j\rangle\Delta\varepsilon_\alpha^{SIC}. \tag{4.24}$$

Since the eigenvalue shift will be negative, this means that we move down the eigenvalues of the selected linear combinations of by an amount $\Delta\varepsilon_\alpha^{SIC}$ and leaves the remainder of the α shell untouched.

4.4.4 The basis set

As described in Chapter 3, the LMTO basis set is generated from the atomic potential at a representative energy for the band to be as close to the final solution as possible. In the full-potential LMTO method we do not employ a minimal basis, and we are in principle free to retain the basis functions obtained from the LDA calculation to expand our solutions, or we may choose to construct the LMTO using the corrected potential, $V^{LDA}(r) - V^{SIC}(r)$, and choose the linearisation to be ε_α^{SIC}. As implemented, the same basis functions will be used *both* for the corrected and the uncorrected states. This should

not cause any major problems, since we can add more basis functions, and in cases of doubt, such as if there are major occupancy of both the itinerant and the localised states, the total energy criterion can be used to determine which is the more favourable.

It seems natural to assume that the optimal choice is to use corrected basis functions, at least for compounds like rare earths where nearly all of the occupation of the shell comes from the corrected states. In practice, however, it has turned out that the best solution has always been to use the LDA basis functions, linearised around the centre of the occupied band, e.g. $E_{t;\ell} \approx \varepsilon_\alpha^{SIC}$. This has given both lower total energies and better numerical stability and convergence properties of the SCF cycle.

4.4.5 SIC density and total energy

To evaluate the SIC total energy in Equation (4.7) we need to project out the density from each of the α-states that were chosen. This is done by applying the projection (4.12), described in connection with the unified Hamiltonian method, to the density matrix calculated as in Equation (3.43),

$$\rho_{ij}^{\alpha}(\mathbf{k}) = \frac{1}{2}\sum_{n} \left(\alpha_{i,n}\rho_{n,j}(\mathbf{k}) + \rho_{i,n}(\mathbf{k})\alpha_{n,j}\right). \tag{4.25}$$

Here we have given the projectors basis function indices, (i, j), to make explicit that we identify the $|m_\ell, \sigma\rangle$ states with specific basis functions. We then proceed as in Equations (3.40-3.42) using the partial density matrices, $\rho_{ij}^{\alpha}(\mathbf{k})$, to obtain the SIC density resolved in lattice harmonic functions

$$n_t^{\alpha}(\mathbf{r}) = \sum_h n_{ht}^{\alpha}(r) D_{ht}(\hat{\mathbf{r}}). \tag{4.26}$$

The Hartree energy can be evaluated for this density by the same methods as for the regular density. For the exchange-correlation energy it has been found that the highly non-spherical form of the density, $n_\alpha^{SIC}(\mathbf{r})$ that results from choosing a crystal field state makes the projection onto crystal harmonic components as described in Equation (3.51) poorly convergent in ℓ_h. To improve the convergence in harmonic functions it is necessary to construct and evaluate the integral,

$$E^{XC}[n_\alpha^{SIC}(\mathbf{r})] = \int d\mathbf{r}\, n_\alpha^{SIC}(\mathbf{r})\, \epsilon^{XC}[n_\alpha^{SIC}(\mathbf{r})], \tag{4.27}$$

directly on the real space (r, θ, ϕ) mesh.

As explained in subsection 3.5.1, the kinetic energy needs to be modified for the extra potential, V^{SI}, applied. In this case Equation (3.53) is given by,

$$T^{corr} = -\sum_{\alpha} \int d\mathbf{r}\, V^{SI}(\mathbf{r}) n^{SIC}(\mathbf{r}) = -\sum_{\alpha} \Delta\varepsilon_{\alpha}^{SIC}, \tag{4.28}$$

which gives an additional contribution to the total energy.

4.4.6 Results

4.4.6.1 Core SIC

A set of tests were done using the core SIC implementation, to check the method against the original results of Perdew and Zunger[54]. The original publication used an atomic solver with no relativistic corrections, whereas the present implementation has a fully relativistic solver. This affects the results, as shown in Table 4.4.6.1. The non-relativistic results of Reference [54] show SIC as giving a drastic improvement over the LDA results, but including relativistic effects we see that for the heavier elements the situation is reversed: SIC overcompensates the LDA error.

Table 4.1: *Comparison of calculated ground state energies using LDA and SIC to experiment for hydrogen and the first noble gases. The discrepancies from the results of Perdew and Zunger[54] are due to the use of a fully relativistic solver for the atomic problem. All numbers are in eV.*

Atom	E^{LDA}	E^{SIC}	E^{LDA}[a]	E^{SIC}[a]	Expt.[b]
H	-13.28	-13.61	-13.28	-13.61	-13.61
He	-77.28	-79.44	-77.1	-79.0	-79.02
Ne	-3493.2	-3521.9	-3488.9	-3517.6	-3508.1
Ar	-14362.4	-14430.3	-14310.5	-14378.3	-14354.6

[a] Calculation of Perdew and Zunger[54].
[b] Veillard and Clementi[71].

It is possible that the result might be improved upon by improving on the choice of single particle state. According to Perdew and Zunger, any single-electron state is completely spin polarised, but this is only true for non-relativistic systems. If we instead as our single-particle states chose for example one of the spin-orbit eigenstates in the $2p_{1/2}$ manifold, there would be no spin polarisation at all. A better model could be constructed by using a polarisation $0 \leq \zeta \leq 1$, determined in some way by the relative strengths of the exchange and spin-orbit interactions.

4.4.6.2 Valence SIC

To compare the method with earlier results we performed calculations for the cubic transition metal oxides[64, 66] and for the first three rare earth elements, Ce, Pr and Nd. The calculations for the transition metal oxides show that the metallic LDA solution is stable for the first two oxides, TiO and VO, but that the insulating SIC solution is favourable for the later oxides in agreement with experimental findings and earlier results with SIC. For the rare earths Pr and Nd we find phase transitions from a localised fcc-like phase to a delocalised α-U phase in rough agreement with experimental findings and in very good agreement with previous SIC calculations[65]. For Ce, the localised γ-phase and the delocalised α-phase can be modelled by the SIC and LDA solutions, respectively. However, the energetics of the two phases come out less favourable in comparison to experiments than earlier SIC calculations[67, 63]. This difference appears to be a consequence of the full-potential scheme, most likely from the use of additional basis functions. Test calculations was attempted as close to an ASA calculation as the method allows, but failed to converge, so it is hard to ascertain exactly were the difference lies.

Another important aspect of the full potential scheme is the finding that in order to give a useful scheme the charge densities of the corrected states needs to be sphericalised. This is in accord with earlier SIC findings[28, 75].

4.4.7 Paper II. CeOFeAs under pressure

In the last year a new group of high-T_C superconductors, iron pnictide superconductors, has been the focus of enormous research efforts. The most successful formula for superconducting properties can be written $REO_{1-x}F_xFeAs$, where RE is a rare earth compound and the structure has been doped with flourine to add extra carriers to the FeAs subsystem. One particular parent compound, CeOFeAs, was studied using the new full-potential implementation of SIC, and it was found that under pressure it should undergo a Mott transition, such that the CeO subsystem becomes metallic.

5. Magnetism

5.1 Non-collinear magnetism and spin spirals

When superimposing any magnetic structure more complex than ferromagnetic ordering on a Bravais lattice, the symmetry of the lattice is destroyed. For a simple anti-ferromagnet this typically doubles the size of the unit cell in some direction, which typically causes no major problem for calculations. But much more complex arrangements can of course be constructed, where the local moments point e.g. in towards some particular site in the unit cell or at right angles to each other, etc. and we then have *non-collinear* magnetic ordering.

One particular form of non-collinear magnetism is the spin spiral, where the directions of the local moments form a spiral along some direction, as illustrated in Figure 5.1. A spiral that repeats itself after N unit cells of the underlying lattice will as for the simple anti-ferromagnet result in an N times bigger supercell. However, if the spiral is incommensurate with the underlying lattice, there is no longer any translation vector that will leave the lattice invariant, and the Bloch description breaks down.

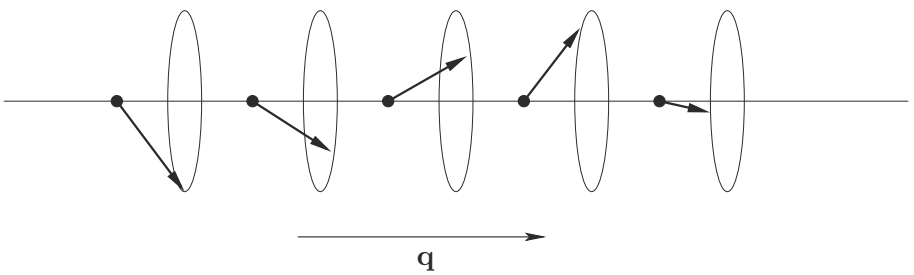

Figure 5.1: A spin spiral illustrated along some array of atoms in a crystal parallel to the spin spiral propagation vector, $\mathbf{q}$. The lattice is no longer invariant under pure translations along this axis, but instead under a translation along the array, $\mathbf{r} \rightarrow \mathbf{r}+\mathbf{R}$, combined with rotation by an angle, $\phi = \mathbf{R} \cdot \mathbf{q}$.

Fortunately, in the case of a spin spiral it is possible to construct a generalised version of Blochs theorem that will restore the unit cell of the non-magnetic lattice[55, 56]. While a lattice exhibiting a spin spiral is not invariant under pure translations, it is invariant under a *combined* translation and rotation of the spins. In general, the angle is given by $\phi = \mathbf{q} \cdot \mathbf{R}$, where $\mathbf{R}$ is the translation vector and $\mathbf{q}$ is the propagation vector of the spin spiral, as il-

lustrated in Figure 5.1. This allows for a generalisation of Bloch's theorem, Equation (2.2), in which we have the wavefunctions,

$$\psi_{\mathbf{k}}(\mathbf{r}) = e^{i\mathbf{k}\cdot\mathbf{r}} \begin{pmatrix} e^{-i\mathbf{q}\cdot\mathbf{r}/2}\,\psi^{\uparrow}_{\mathbf{k}}(\mathbf{r}) \\ e^{i\mathbf{q}\cdot\mathbf{r}/2}\,\psi^{\downarrow}_{\mathbf{k}}(\mathbf{r}) \end{pmatrix}. \tag{5.1}$$

If the Hamiltonian is diagonal in spins it will commute with a combined translation-rotation as described above. Then Equation (5.1) merely expresses a rotation of the solutions in each k-point of the Brillouin zone, and there is no need to extend the calculation to larger cells either in k-space or in real space. This puts restrictions on the Hamiltonians that can be used, most notably, spin-orbit interaction cannot be included at the same time as a spin spiral is described by the generalised Bloch theorem.

5.2 Paper III. The incommensurate magnetic structure of $TbNi_5$

The compound $TbNi_{5-x}Cu_x$ were synthesised and characterised for concentrations, $x = 0, 0.5, 1.0, 1.5, 2.0$. The magnetic structure of all the copper substituted compounds is ferromagnetic, but the pure $TbNi_5$ system has a helical spiral with a propagation vector $\mathbf{q} = (0, 0, 0.0195)$. The magnetic moment measurements show that the f-electrons of Tb are localised in an f^8 configuration.

Electronic structure calculations using the full-potential LAPW and TB-LMTO methods were performed for the unalloyed ($x = 0$) structure, in order to characterise the mechanism of the non-collinear magnetic ordering. The f-electrons of Tb were treated in the open core approximation, removing them from the valence band, but allowing for a spin splitting of the valence band through the coupling via the exchange-correlation potential. The calculations could not resolve the very small ordering vector in total energy. However, a Fermi surface analysis reveals the possibility of Fermi surface nesting between the spin up and spin down bands, which by the Fermi level are split by a small amount by the local moment from the f-electrons.

5.3 Paper IV. Non-collinear structure of $CeRhIn_5$

The heavy fermion compound $CeRhIn_5$ has attracted a lot of attention because it shows a coexistence of superconductivity and an ordered anti-ferromagnetic phase. It is a tetragonal compound, with the moments ordered anti-ferromagnetically in the ab plane, and the direction of the magnetisation of these planes is described by a spiral along the c-axis. The spin spiral propagation vector is $\mathbf{q} = (1/2, 1/2, q_z)$, with $q_z = 0.298$. There

has been some controversy over whether the $4f$ electron of the Ce atom is localised or delocalised in this compound, but Fermi surface data and calculations suggests that the localised solution is the preferable one.

To analyse the magnetic state of $CeRhIn_5$ we performed calculations both using an open core treatment of the Ce $4f$ electron and using LDA+U. The open core calculations failed to resolve the small energy differences involved, but in the LDA+U approach we did indeed find a spin spiral with a propagation vector $\mathbf{q} = (1/2, 1/2, 0.375)$. An analysis of the Fermi surface revealed a large nesting corresponding to this wave vector and, we therefore attribute this breaking of the crystal symmetry to Fermi surface nesting.

5.4 Paper V. $FeMnSi_{0.75}P_{0.25}$

The magnetic structure of hexagonal $FeMnSi_{0.75}P_{0.25}$ was found to be very sensitive to the precise details of the synthesis. If the melt is annealed slowly, the sample becomes an anti-ferromagnet, whereas if it is quenched, it becomes a ferromagnet with a magnetic moment of $1.26\mu_B$. Characterisation of the samples using X-ray diffraction and Mössbauer spectroscopy reveals no other difference of the structures than a slight increase in the disorder of the Fe-Mn sites for the quenched sample.

Theoretical calculations where carried out using the EMTO method[72], and the coherent potential approximation (CPA) was used to simulate the disorder of the Fe-Mn sublattice. The results indicate that the magnetic ordering of the quenched sample is not a pure ferromagnet but a ferrimagnet, with Fe and Mn atoms coupling antiferromagnetically.

6. Paper VIII. The $5f$ electron occupation of Pu from XPS

Plutonium has one of the most complex phase diagrams of all the elements. At ambient pressure, it undergoes six phase transformations as function of temperature before melting, the volumes of the different phases are very different, and several of them exhibit anomalous behaviour such as negative temperature expansion. These difficulties have spurred large efforts in the electronic structure community to find a theory capable of simultaneously describing all these properties.

The development of more sophisticated techniques in electronic structure theory also advances the need for evaluation of the results obtained in terms of experimental quantities. One useful and easily obtained quantity in electronic structure calculations are partial occupancies of some orbital shell. These are particularly useful, since many of the extensions to regular DFT in the Kohn-Sham picture, such as SIC, LDA+U or orbital polarisation, are schemes that explicitly manipulate these shells and their occupancies. Unfortunately partial occupancies of specific shells are not directly observables, and so indirect ways of deriving values for them from experiments must be used. In Paper VIII we attempt to establish a relation between the $5f$ occupation and the $4f$ core binding energy.

6.1 X-ray photoelectron spectroscopy

Before proceeding to the result of the investigation, we will very briefly review the experimental technique X-ray photoelectron spectroscopy (XPS)[60, 52], and in particular, explain the phenomenon of well screened and poorly screened features of the spectrum. XPS is a well established method for determining binding energies in solids.

An incoming photon ionises one of the orbitals of an atom in the solid. This leads to an electron being expelled from the solid with a kinetic energy, $E_K = \hbar\omega - \phi - E_B$, where we have the photon energy, $\hbar\omega$, the work function, ϕ, and the binding energy of the electron, E_B. The binding energy is defined as the energy difference of the ionised and the unionised atom, $E_B = E_{A^+} - E_A$. The energy of the ionised system, E_{A^+}, is known as the final state energy and it should be noted that the + sign is a superscript noting that when an electron leaves a localised orbital a positive ion is left as an impurity in the solid. An

illustration of the process resulting in a measured spectrum is shown in Figure 6.1. As the incoming photon energy can be controlled with great accuracy and the work function is just a constant, the kinetic energy of the photons directly measure the binding energy of the electrons.

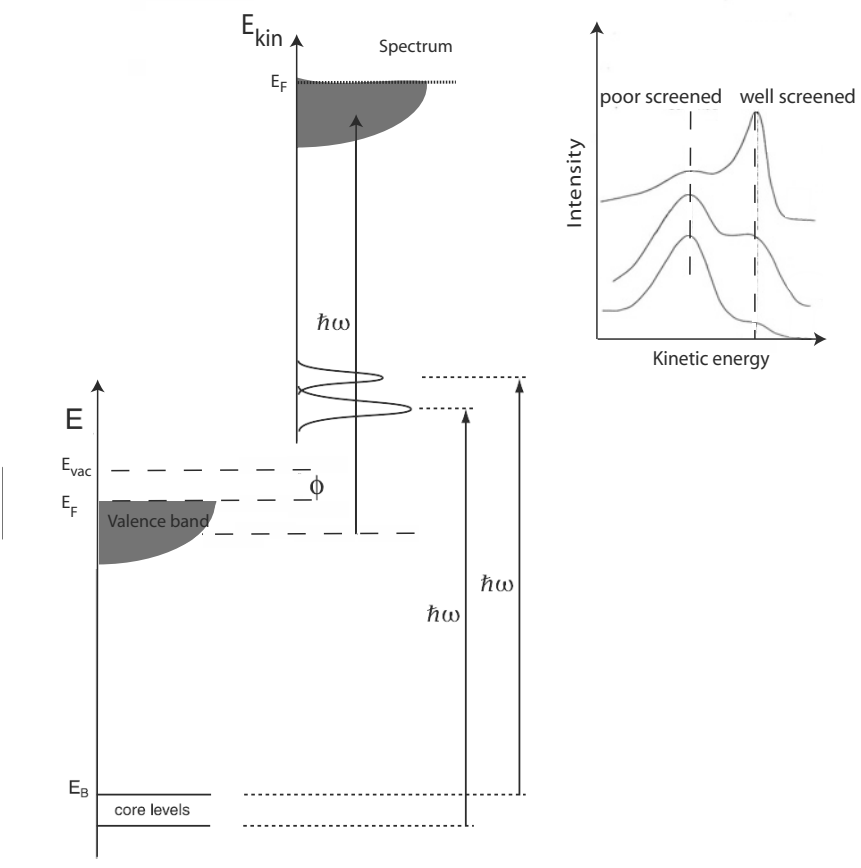

Figure 6.1: The principle of XPS. A photon of energy $\hbar\omega$ ionises an orbital with binding energy $E_K = \hbar\omega - \phi - E_B$. The inset shows examples of well screened and poor screened features of electron spectroscopy, adapted from data of Fuggle et al.[22] The top curve represents a material with itinerant valence band f-states, whereas in the bottom curve these states are localised. The curve in the middle represents an intermediate case.

The XPS process has an ionised system as a final state, where primarily the core hole provides the main difference in electronic structure compared to the unionised system. The absence of the core electron provides an additional positive charge which attracts electrons to it, a process known as the screening of the core hole. Details in how this screening process appears result in a variety of binding energies, due to different values of the final state

energy energy, E_{A^+}. The standard theory for core hole screening in solids was developed by Gunnarsson and Schönhammer[27], consisting of the analysis of an Anderson-like many-body Hamiltonian. One of its consequences, in its standard interpretation, is that multiple screening channels can exist simultaneously in a solid. This means that a single core level excitation may leave more than one peak in the XPS spectrum, as the different screening channels result in different binding energies. A schematic picture of this fact is shown in the inset of Figure 6.1. If the screening electron is due to narrow band states at the Fermi level of the same angular momentum as the core hole, the screening is efficient and results in the outgoing electron seeing less of the positive core, resulting in a high kinetic energy. If, on the other hand, the screening orbital is a broad band state, preferably of an angular momentum character different than that of the core hole, the screening is less efficient and the electron will leave the material with a smaller kinetic energy. These peaks are thus traditionally referred to as the "well screened" and "poor screened" peaks, respectively.

In lanthanide and actinide compounds the well and poor screened peaks can be directly coupled to the degree of localisation of the valence band f shell. The f electrons of itinerant states make narrow bands close to the Fermi level that will be responsible for efficient screening, and one observes a pronounced well screened peak. For a material with a localised f-electron valence band, these valence electrons have been pulled away from the Fermi level, leaving only the spd electrons to perform the screening, and one typically observes a poor screened peak.

6.2 Results

We have studied Pu compounds where a reliable $5f$ count can either be established on the basis of experiments such as magnetometry, resistivity measurements or neutron scattering experiments or, for the oxides and very highly oxidised compounds, according to the formal oxidation number. We obtain $4f$ core binding energies of plutonium in a number of compounds from previously published XPS data. The result is displayed in Figure 6.2 and, along with references to the sources, in Table 6.1.

The main conclusion drawn from this data is that all phases of metallic Pu has a $5f$ occupation of close to 5 electrons. A significant deviation from this would result in a shift of the core binding energies, which is not observed; only a redistribution from the well screened to the poorly screened features are seen, which shows the variation of the localisation of the $5f$ electrons.

A particularly problematic compound in the study is PuN. It is not clear what designation is the appropriate one, but to fit in the present diagram, it must be considered to be either in a f^4 or f^6 configuration. Valence spectroscopies of PuN show a three-peak structure[31] which is interpreted as a

$f^6 \rightarrow f^5$ transition could be indication of an f^6 configuration. On the other hand, available neutron data[12] suggests an f^4 configuration, and generally we expect the f^5 to be stable in metallic systems[39]. It is at present not clear how to interpret and reconcile these seemingly contradictory facts.

Table 6.1: *Excitation energies for Pu $4f$ states (in eV), and designation of oxidation states*.

	Poor screened		Well screened		
	$4f_{5/2}$	$4f_{7/2}$	$4f_{5/2}$	$4f_{7/2}$	Oxidation state
Pu[44]			434.9	422.2	
α-Pu[10]			435.1	422.1	
α-Pu[2, 18, 19]			435.2[1]	422[1]	
β-Pu[2, 18]			435.2[1]	422[1]	
γ-Pu[2, 18]			435.2[1]	422[1]	
δ-Pu[2, 18]			435.2[1]	422[1]	
Pu[31]	437.5	424.6			
Pu Suboxide[44]	437.1	424.4			(III)
Pu_2O_3[16]	437.2	424.5			(III)
PuO_2[70]	439.3	426.6			(IV)
PuO_2[44]	438.7	426.1			(IV)
PuO_2[16]	438.6	426			(IV)
$Pu(OH)_4$[19]	439.5[1]	426.6			(IV)
$Pu(NO_3)_4 \cdot nH_2O$[69]	439.8	427.1			(IV)
PuO_2CO_3[19]	441.1[1]	428.8			(VI)
$Cs_2PuO_2Cl_4$[68]	441.2	428.7			(VI)
PuH_2[45]		425.0			(III)
PuSe[25]	437.6	424.7		420.6	(III)[20]
PuSb[25]	437.7	424.9			(III)[73]
PuN[31]	(436.3?)	(423.6?)	436.3	423.6	(III)[73]
$PuFe_2$[24]	437.8[1]	424.6[17]		422.6	(III)[77]
$Pu_{1-x}Am_x$[9]	The same as for metallic plutonium				

[1]Estimated from the figures of the original references.

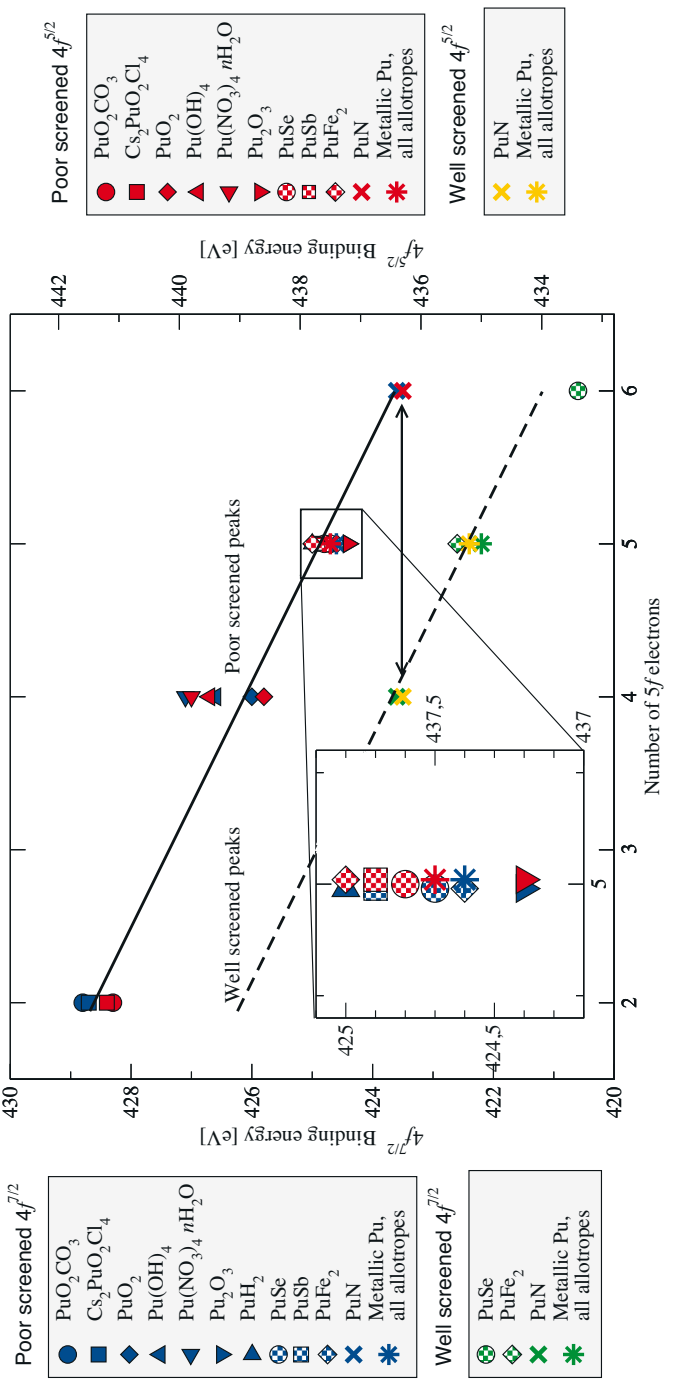

Figure 6.2: Pu $4f$ core shifts as function of $5f$ occupancy.

7. Outlook and conclusions

The work presented in this thesis has taken us to a point that is, hopefully, slightly higher up than we were before, and here is now presented a small collection of thoughts on the view of the world from this point. It will perhaps seem a bit negatively biased, since it consists of thoughts about some rather difficult things that are part of the everyday work with the methods of electronic structure calculations, such as trying to establish the errors of our calculations. Despite the very large fraction of the total time spent working on a problem that is taken up by such questions they often are a very small part of published papers, and this little discussion therefore seems appropriate here.

While SIC in the full-potential scheme retains its strong points in that the good total energy, compatible with the LDA energy and free of the double counting problem that plagues for example LDA+U, the need to require that we restrict ourselves to only the spherical component of the correction is problematic. Nothing in the basic argument for the form of the self-interaction gives any reason for such a restriction. The error (if such it be) comes from the evaluation of the XC energy, which behaves in a very non-linear fashion for a highly non-spherical charge density. An interesting thing to note is that the Lundin-Eriksson formulation of SIC[49] evaluates the total density, which is large and rather spherical, minus the non-spherical density of the corrected state. This difference should still be rather spherical, and so the problem might not arise in this scheme. Another interesting question is what impact the gradients of a GGA scheme would have on the non-spherical part of the correction. Further studies of the non-spherical contributions to the self-interaction are needed to better judge how well-founded the theory actually is.

The two last papers concern two important issues, the dependence of our end result on various parameters that we specify ourselves, and more generally how we determine if the results are correct. Paper VIII attempts a straightforward determination of a common parameter from experiment and theory that can be compared, and such comparisons are of course usually done in any theoretical study to ascertain the validity of the results. Still, more such numbers are needed when we wish to extend DFT to more correlated systems. The present approximations in this field (SIC, LDA+U, orbital polarisation...) are still at a rather crude stage, heavily dependent on details of implementations and arbitrary choices of the practitioner. They all have a long way to go before approaching the accuracy of regular DFT schemes.

In Paper VII, we are concerned, in a small way, with questions of how we can ascertain that the first principles result really is *in itself* correct. In other words, do our calculation really produce the answer that the theoretical model should give. In the first principles community the claim is often heard that we have the tools to make quantitative as well as qualitative predictions, yet quantitative estimates of errors for calculated values are too often absent in papers. The present work admittedly no exception to this, and the main reason is quite clearly the exchange-correlation functionals which introduce errors that are very hard to estimate quantitatively. Nevertheless, it is felt that questions of the quantitative accuracy of our schemes is presently one of the large challenges in the field.

8. Populärvetenskaplig sammanfattning på svenska

De flesta av vår vardag bestäms av elektronstrukturen hos olika material. Påståendet kan tyckas överaskande, men det ligger en stor del sanning i det. Solens strålar får i och för sig sin energi från kärnreaktioner, men när vi känner hur de värmer vår hud är det för att elektronstrukturen i några nervändar registrerar värmen, och på vägen har atmosfärens molekyler genom in elektronstruktur filtrerat bort våglängder som skulle ha skadat oss. Tack vare elektronstrukturen i koppartråden har vi elektricitet i våra hem, elektronstrukturen för ett kylmedium ser till att det går att transportera värme ut ur kylskåpet och kylskåpsmagnetens elektronstruktur ser till att den sitter fast på kylskåpsdörren. Och så kan man fortsätta att rada upp exempel.

Vi tänker förstås inte på företeelser som känslan av värme i huden som en elektronstruktureffekt Det är inte särskilt troligt att ens en ingenjör som konstruerar kylskåp funderar närmare över kylmediets elektronstruktur, men i grundforskningen om materials egenskaper är elektronstrukturen en hörnsten för vår förståelse.

I den här avhandlingen studeras i huvudsak magnetiska egenskaper och kristallers struktur, och det sammanhållande temat är de så kallade f-elektronsystemen. f-elektronsystemen består av två klasser av ämnen, lantanider och aktinider, och den som känner till det periodiska systemet känner igen dem som de två raderna längst ner som ställts ut lite åt sidan. Ämnena har i sina yttersta elektronskal så kallade f-elektroner, vilka ger materialen en stor mängd fascinerande egenskaper, men som också är en stor utmaning för beräkningar och modeller.

Den övergripande metod som använts i studierna är densitetsfunktionalteori, ett sätt att beskriva elektronstrukturen med hjälp av bara elektrontätheten i kristallen. Utifrån denna kan man konstruera Kohn-Sham-ekvationen, en sorts hjälpsystem för att lösa kvantmekanikens huvudekvation, Schrödingerekvationen, för ett system av elektroner som alla växelverkar med varandra. Med detta angreppssätt krävs att man har någon form av approximation som för en elektron i materialet beskriver effekten av alla de andra elektronerna, en beskrivning av hur en elektron ”ser” molnet av alla andra elektroner.

Ett problem som uppstår i de vanligaste approximationerna till denna växelverkan är att när man lägger ihop effekterna av alla andra elektroner så kommer elektronen vi är intresserade av själv med. Detta leder till att varje elek-

tron i materialet i viss mån kommer att växelverka med sig själv. Denna extra självväxelverkan är i de flesta fall så liten att den inte är ett problem, men i de fall då en elektron är benägen att sitta på en viss atom utan att röra sig så mycket i kristallen kan den felaktiga självväxelverkan bli stor. Som en liten baron von Münchhausen, som lyfte sig själv i håret ur träsket, lyfter sig elektronen själv upp från att sitta bunden vid en atom och börjar röra sig i materialet, vilket ger felaktiga resultat i våra beräkningar. I avhandlingen beskrivs hur en metod som korrigerar det här beteendet, självväxelverkanskorrektion har utvecklats för en specifik elektronstrukturmetod. Metoden har också använts för att studera ett nyupptäckt supraledande material, CeOFeAs.

De flesta associerar säkert magnetiska material till föremål som den tidigare nämnda kylskåpsmagneten. Den är fall där alla atomerna riktar sin magnetisering åt samma håll, ett ferromagnetiskt material. Detta är inte det enda möjliga tillståndet, naturen förser oss med en förbluffande rik flora av magnetiska strukturer. Atomernas magnetisering i stället kan peka i motsatta riktningar från en atom till nästa, vilket är ett enkelt fall av antiferromagnetism. Som antiferromagnetism benämns också ett tillstånd då flera atomers moment pekar in mot en annan atom, eller vrider sig från ett atomlager till nästa som en spiral. Det sistnämnda kallas också spin-spiral och är en av de magnetiska strukturer som särskilt har studerats i två av studierna i avhandlingen.

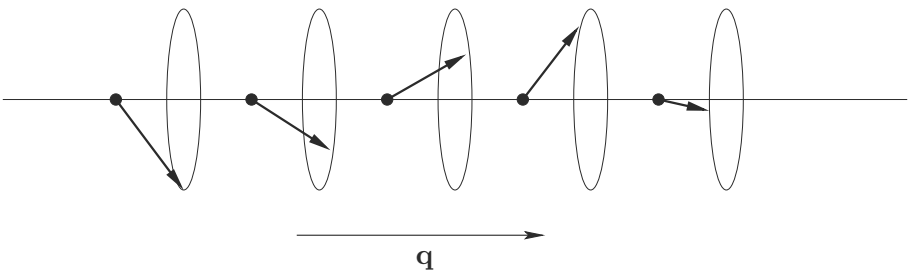

Figure 8.1: Illustration av en spin-spiral, en av de magnetiska strukturerna som studerats i avhandlingen.

Vad som händer med material vid höga temperaturer har också studerats med en förbättrad metod för att beskriva vibrationerna i materialet, de så kallade fononerna. Om fononerna tillåts växelverka med varandra på ett sätt som påminner om det som beskrevs tidigare för elektronerna kan man visa att vibrationerna själva kan stabilisera vissa kristallstrukturer.

De sista två artiklarna i avhandlingen försöker på olika sätt bedömma och förbättra själva elektronstrukturmetoderna. Den ena är en studie av experimentella data för att försöka fastställa antalet f-elektroner i grundämnet plutonium i fast form. Detta är gjort som en hjälp för att bedöma kvaliteten i olika approximationer för beräkning av elektronstrukturen. I den andra har ett förbättrat schema för den så kallade Brillouinzonsintegrationen tagits fram och testats.

9. Acknowledgements

It is curious that when you try to sum up what is supposedly your great achievement what strikes you most is how grateful you are to a lot of people. This thesis is no exception. There are many people who have contributed to the final form of this thesis and I am sure that now in as the deadline fast approaches my fingers will accidentally slip and forget someone. My apologies if that happens. My warmest thanks to:

My supervisor Olle Eriksson for the opportunity to come to Uppsala and write this thesis. It has been a tremendous inspiration to work with you.

My other two supervisors, Per Andersson and Lars Nordström for always taking their time for my more or less crazy thoughts, Per with his endless enthusiasm and Lars with his soberingly sceptical Look. I am not sure how I will manage without those things, but I guess I will have to try.

John Wills for the times in Los Alamos and all the wisdom of electronic structure calculations that I owe to those visits that helped me become one of the many people indebted to him for letting us build on his fantastic code.

Börje Johansson for always being ready with a big smile to show us all that being a successful scientist does not mean being unhappy.

Olof ”Charlie” Karis for help with the XPS figure.

Elisabeth Bill for somehow ensuring that bureaucratic problems just don’t seem to exist.

Peter Larsson for making the computers go and for all discussions. I am convinced the world would be a better place if we had designed it from scratch.

The DMFT gang – Igor, Oscar and Patrik – for always being ready for another fight over physics and coding.

Lars B for getting me started.

Petros and Bulten, my fellow players in Fysik 4’s Förnedringsorkester.

Everyone else at Fysik 4/Theoretical magnetism/Materials theory . . . sorry that I don’t have time to name you all, but I really have to run with this to the printers now. You are all great!

Tomas Hässler for patiently explaining why the c-compiler is right and I am wrong.

My parents-in-law Hans and Riita for the child free time in their cellar that saw me through several of the chapters the thesis.

My parents for encouraging me.

My wife Heidi and daughter Hillevi for always being ready to show me that physics is not as important as all that.

Bibliography

[1] `http://www.rspt.net`.

[2] J. W. Allen, Y.-X. Zhang, L. H. Tjeng, L. E. Cox, M. B. Maple, and C.-T. Cheng. Photoemission and inverse photoemission studies on actinide metals – does any model work? *Journal of Electron Spectroscopy and Related Phenomena*, 78:57–62, 1996.

[3] O. K. Andersen. Linear methods in band theory. *Physical Review B*, 12(8):3060–3083, Oct 1975.

[4] O. K. Andersen, C. Arcangeli, R. W. Tank, T. Saha-Dasgupta, G. Krier, O. Jepsen, and I. Dasgupta. Third-generation TB-LMTO. In C. L., G. A., and T. P., editors, *Tight-Binding Approach to Computational Materials Science*, pages 3–34, Pittsburgh, 1998. Materials Research Society.

[5] O. K. Andersen and O. Jepsen. Explicit, first-principles tight-binding theory. *Physical Review Letters*, 53:2571, Dec 1984.

[6] V. I. Anisimov, J. Zaanen, and O. K. Andersen. Band theory and Mott insulators: Hubbard U instead of Stoner I. *Physical Review B*, 44(3):943–954, Jul 1991.

[7] R. Armiento and A. E. Mattsson. Functional designed to include surface effects in self-consistent density functional theory. *Physical Review B*, 72(8):085108, Aug 2005.

[8] N. W. Ashcroft and N. D. Mermin. *Solid State Physics*. Harcourt College Publishers, Fort Worth, 1967.

[9] N. Baclet, M. Dormeval, L. Havela, J. M. Fournier, C. Valot, F. Wastin, T. Gouder, E. Colineau, C. T. Walker, S. Bremier, C. Apostolidis, and G. H. Lander. Character of 5f states in the Pu-Am system from magnetic susceptibility, electrical resistivity, and photoelectron spectroscopy measurements. *Physical Review B*, 75(3):035101, 2007.

[10] R. Baptist, D. Courteix, J. Chayrouse, and L. Heintz. X-ray photoemission study of plutonium metal. *Journal of Physics F*, 12(9):2103–2114, 1982.

[11] P. Blöchl, O. Jepsen, and O. Andersen. Improved tetrahedron method for Brillouin-zone integrations. *Physical Review B*, 49:16223, Jun 1994.

[12] A. Boeuf, R. Caciuffo, J. M. Fournier, L. Manes, J. Rebizant, E. Roudaut, and F. Rustichelli. ^{239}pun powder neutron diffraction study. *Solid State Communications*, 52(4):451 – 453, 1984.

[13] T. Burkert. *Materials for Magnetic Recording Applications*. PhD thesis, Uppsala University, Department of Physics, 2005.

[14] D. M. Ceperley and B. J. Alder. Ground state of the electron gas by a stochastic method. *Physical Review Letters*, 45(7):566–569, Aug 1980.

[15] E. U. Condon and G. H. Shortley. *The theory of atomic spectra*. Cambridge University Press, Cambridge, 1935.

[16] D. Courteix, J. Chayrouse, L. Heintz, and R. Baptist. XPS study of plutonium oxides. *Solid state communications*, 39:209–213, 1981.

[17] L. E. Cox. X-ray photoemission study of $\delta - Pu$ stabilized by 1 wt.% Ga: Electronic structure and sputter-induced surface phase transformation. *Physical Review B*, 37(14):8480–8483, May 1988.

[18] L. E. Cox, J. M. Peek, and J. W. Allen. Pu 4f XPS spectra analyzed in the Anderson impurity model. *Physica B*, 259-261:1147–1148, 1999.

[19] J. D. Farr, R. K. Schulze, and M. P. Neu. Surface chemistry of Pu oxides. *Journal of Nuclear Materials*, 328:124–136, 2004.

[20] J. M. Fournier, E. Pleska, J. Chiapusio, J. Rossat-Mignod, J. Rebizant, J. E. Spirlet, and O. Vogt. Electrical resistivity of plutonium monochalcogenides. *Physica B*, 163:493–495, 1990.

[21] S. Froyen. Brillouin-zone integration by Fourier quadrature: Special points for superlattice and supercell calculations. *Physical Review B*, 39(5):3168–3172, 1989.

[22] J. C. Fuggle, M. Campagna, Z. Zolnierek, R. Lässer, and A. Platau. Observation of a relationship between core-level line shapes in photoelectron spectroscopy and the localization of screening orbitals. *Phys. Rev. Lett.*, 45(19):1597–1600, Nov 1980.

[23] R. Gaspar. Über eine Approximation des Hartree-Fockschen Potentials durch eine universelle Potentialfunktion. *Acta Physica Academiae scientiarum Hungaricae*, 3:263–285, 1954.

[24] J. Ghijsen. Photoemission study (xps, ups) of $pufe_2$. *Journal of Electron Spectroscopy and Related Phenomena*, 35:19–26, 1985.

[25] T. Gouder, F. Wastin, J. Rebizant, and L. Havela. $5f$-electron localization in PuSe and PuSb. *Physical Review Letters*, 84(15):3378–3381, Apr 2000.

[26] O. Gunnarsson, A. V. Postnikov, and O. K. Andersen. Density-functional calculation of effective Coulomb interactions in nonmetallic systems: Application to Mn in CdTe, CdS, and ZnO. *Physical Review B*, 40(15):10407–10411, Nov 1989.

[27] O. Gunnarsson and K. Schönhammer. Co on cu(100)—explanation of the three-peak structure in the x-ray-photoemission-spectroscopy core spectrum. *Physical Review Letters*, 41(23):1608–1612, Dec 1978.

[28] J. G. Harrison. An improved self-interaction-corrected local spin density functional for atoms. *Journal of Chemical Physics*, 78(7):4562, April 1983.

[29] W. A. Harrison. *Solid state theory*. Dover, New York, 1979.

[30] D. R. Hartree. The wave mechanics of an atom with a non-coulomb central field. part i. theory and methods. *Mathematical Proceedings of the Cambridge Philosophical Society*, 24(01):89–110, 1928.

[31] L. Havela, F. Wastin, J. Rebizant, and T. Gouder. Photoelectron spectroscopy study of PuN. *Physical Review B*, 68:85101, 2003.

[32] R. A. Heaton, J. G. Harrison, and C. C. Lin. Self-interaction correction for energy band calculations: Application to LiCl. *Solid State Communications*, 41(11):827–829, March 1982.

[33] R. A. Heaton, J. G. Harrison, and C. C. Lin. Self-interaction correction for density-functional theory of electronic energy bands of solids. *Physical Review B*, 28:5992–6007, 1983.

[34] L. Hedin. New method for calculating the one-particle green's function with application to the electron- gas problem. *Physical Review*, 139:A796, Jan 1965.

[35] P. Hohenberg and W. Kohn. Inhomogeneous electron gas. *Physical Review*, 136(3B):B864–B871, Nov 1964.

[36] J. D. Jackson. *Classical electrodynamics*. Wiley, New York, 3rd edition, 1999.

[37] J. F. Janak. Proof that $\partial e/\partial ni = \epsilon$ in density-functional theory. *Physical Review B*, 18(12):7165–7168, Dec 1978.

[38] O. Jepsen and O. K. Andersen. The electronic structure of h. c. p. ytterbium. *Solid State Communications*, 88(11/12):871–875, 1993.

[39] B. Johansson and A. Rosengren. Interpolation scheme for the cohesive energies for the lanthanides and actinides. *Physical Review B*, 11(4):1367–1373, Feb 1975.

[40] C. Kittel. *Introduction to Solid State Physics*. John Wiley & Sons, New York, Chichester, 8 edition, 2005.

[41] D. D. Koelling and B. N. Harmon. A technique for relativistic spin-polarised calculations. *Journal of Physics C*, 10(3107):37, 1977.

[42] W. Kohn and L. J. Sham. Self-consistent equations including exchange and correlation effects. *Physical Review*, 140(4A):A1133–A1138, Nov 1965.

[43] A. Kuznetsov, V. Dmitriev, L. Dubrovinsky, V. Prakapenka, and H. P. Weber. FCC-HCP phase boundary in lead. *Solid State Communications*, 122(3-4):125 – 127, 2002.

[44] D. T. Larson. AES and XPS study of plutonium oxidation. *Journal of vacuum science and technology*, 17(1):55–58, 1979.

[45] D. T. Larson and K. M. Motyl. Detection of plutonium hydride using X-ray photoelectron spectroscopy. *Journal of Electron Spectroscopy and Related Phenomena*, 50:67–76, 1990.

[46] G. Lehmann and M. Taut. On the numerical calculation of the density of states and related properties. *Physica Status Solidi B*, 54:469–477, Jan 1972.

[47] T. L. Loucks. *Augmented plane wave method : a guide to performing electronic structure calculations*. W.A. Benjamin, New York, 1967.

[48] M. Lüders, A. Ernst, M. Däne, Z. Szotek, A. Svane, D. Ködderitzsch, W. Hergert, B. L. Györffy, and W. M. Temmerman. Self-interaction correction in multiple scattering theory. *Physical Review B*, 71(20):205109, May 2005.

[49] U. Lundin and O. Eriksson. Novel method of self-interaction corrections in density functional calculations. *Int. J. Quantum Chem.*, 81(4):247–252, 2001.

[50] M. Methfessel and A. Paxton. High-precision sampling for Brillouin-zone integration in metals. *Physical Review B*, 40:3616–3621, Aug 1989.

[51] H. Monkhorst and J. Pack. Special points for Brillouin-zone integrations. *Physical Review B*, 13:5188, Jun 1976.

[52] C. Nordling, S. Hagström, and K. Siegbahn. Application of electron spectroscopy to chemical analysis. *Zeitschrift für Physik A Hadrons and Nuclei*, 178(5):433–438, 10 1964.

[53] J. P. Perdew, K. Burke, and M. Ernzerhof. Generalized gradient approximation made simple. *Physical Review Letters*, 77(18):3865–3868, Oct 1996.

[54] J. P. Perdew and A. Zunger. Self-interaction correction to density-functional approximations for many-electron systems. *Physical Review B*, 23(10):5048–5079, May 1981.

[55] L. M. Sandratskii. Symmetry analysis of electronic states for crystals with spiral magnetic order. i. general properties. *Journal of Physics: Condensed Matter*, 3(44):8565–8585, 1991.

[56] L. M. Sandratskii. Symmetry analysis of electronic states for crystals with spiral magnetic order. II. connection with limiting cases. *Journal of Physics: Condensed Matter*, 3(44):8587–8596, 1991.

[57] H. L. Skriver. *The LMTO method*. The Springer Series in Solid-State Sciences. Springer, Berlin, 1984.

[58] J. C. Slater. A simplification of the Hartree-Fock method. *Physical Review*, 81(3):385–390, Feb 1951.

[59] J. C. Slater. *The self-consistent field for molecules and solids*, volume 4 of *Quantum theory of molecules and solids*. McGraw-Hill, New York, 1974.

[60] E. Sokolowski, C. Nordling, and K. Siegbahn. Chemical shift effect in inner electronic levels of cu due to oxidation. *Physical Review*, 110(3):776, May 1958.

[61] P. Souvatzis. *Electronic Structure and Lattice Dynamics of Elements and Compounds*. PhD thesis, Uppsala University, Department of Physics, 2007.

[62] P. Souvatzis, O. Eriksson, M. I. Katsnelson, and S. P. Rudin. Entropy driven stabilization of energetically unstable crystal structures explained from first principles theory. *Physical Review Letters*, 100(9):095901, 2008.

[63] A. Svane. Electronic structure of cerium in the self-interaction corrected local spin density approximation. *Physical Review Letters*, 72(8):1248–1251, Feb 1994.

[64] A. Svane and O. Gunnarsson. Transition-metal oxides in the self-interaction-corrected density-functional formalism. *Physical Review Letters*, 65(9):1148–1151, Aug 1990.

[65] A. Svane, J. Trygg, B. Johansson, and O. Eriksson. Electronic-structure calculations of praseodymium metal by means of modified density-functional theory. *Physical Review B*, 56(12):7143–7148, Sep 1997.

[66] Z. Szotek, W. M. Temmerman, and H. Winter. Application of the self-interaction correction to transition-metal oxides. *Physical Review B*, 47:4029, Feb 1993.

[67] Z. Szotek, W. M. Temmerman, and H. Winter. Self-interaction corrected, local spin density description of the $\gamma \rightarrow \alpha$ transition in Ce. *Physical Review Letters*, 72(8):1244–1247, Feb 1994.

[68] Y. A. Teterin and A. Y. Teterin. The structure of X-ray photoelectron spectra of light actinide compounds. *Russian chemical reviews*, 73(6):541–580, 2004.

[69] Y. A. Teterin, A. Y. Teterin, N. G. Yakovlev, I. O. Utkin, K. E. Ivanov, L. D. Shustov, L. D. Vukcevic, and G. N. Bek-Uzarov. X-ray photoelectron study of actinide (Th, U, Pu, Am) nitrates. *Nuclear Technology and Radiation Protection*, 18(2):31–35, 2003.

[70] B. W. Veal, D. J. Lam, H. Diamond, and H. R. Hoekstra. X-ray photoelectron-spectroscopy study of oxides of the transuranium elements Np, Pu, Am, Cm, Bk, and Cf. *Physical Review B*, 15(6):2929–2942, Mar 1977.

[71] A. Veillard and E. Clementi. Correlation energy in atomic systems. v. degeneracy effects for the second-row atoms. *Journal of Chemical Physics*, 49:2415, Jan 1968.

[72] L. Vitos. *Computational Quantum Mechanics for Materials Engineers: The EMTO Method and Applications*. Engineering Materials and Processes Series. Springer-Verlag, London, 2007.

[73] O. Vogt and K. Mattenberger. Magnetic measurements on rare earth and actinide monopnictides and monochalcogenides. In J. K. A. Gschneider, L. Eyring, G. H. Lander, and G. R. Choppin, editors, *Lanthanides/Actinides Physics - I*, volume 17 of *Handbook on the Physics and Chemistry of Rare earths*, pages 301–407, Amsterdam, 1993. North Holland.

[74] U. von Barth and L. Hedin. A local exchange-correlation potential for the spin polarized case: I. *J Phys C: Solid State Phys*, 5:1629, Jan 1972.

[75] O. A. Vydrov and G. E. Scuseria. Ionization potentials and electron affinities in the perdew-zunger self-interaction corrected density-functional theory. *Journal of Chemical Physics*, 122:4107, May 2005.

[76] J. M. Wills, O. Eriksson, M. Alouani, and D. L. Price. Full-potential LMTO total energy and force calculations. In H. Dreussé, editor, *Electronic Structure and Physical Properties of Solids; The Uses of the LMTO Method*, pages 148–167. Springer, 1996.

[77] M. Wulff, G. H. Lander, J. Rebizant, J. C. Spirlet, B. Lebech, C. Broholm, and P. J. Brown. Magnetic moments and Pu form factor in $PuFe_2$. *Physical Review B*, 37(10):5577–5585, Apr 1988.

[78] J. Zabloudil, R. Harmmerling, L. Szunyogh, and P. Weinberger. *Electron Scattering in Solid Matter*. The Springer Series in Solid-State Sciences. Springer, Berlin, 2005.

[79] R. Zeller, P. H. Dederichs, B. Újfalussy, L. Szunyogh, and P. Weinberger. Theory and convergence properties of the screened Korringa-Kohn-Rostoker method. *Physical Review B*, 52(12):8807–8812, Sep 1995.

Acta Universitatis Upsaliensis

Digital Comprehensive Summaries of Uppsala Dissertations from the Faculty of Science and Technology 686

Editor: The Dean of the Faculty of Science and Technology

A doctoral dissertation from the Faculty of Science and Technology, Uppsala University, is usually a summary of a number of papers. A few copies of the complete dissertation are kept at major Swedish research libraries, while the summary alone is distributed internationally through the series Digital Comprehensive Summaries of Uppsala Dissertations from the Faculty of Science and Technology. (Prior to January, 2005, the series was published under the title "Comprehensive Summaries of Uppsala Dissertations from the Faculty of Science and Technology".)

Distribution: publications.uu.se
urn:nbn:se:uu:diva-109639

ACTA
UNIVERSITATIS
UPSALIENSIS
UPPSALA
2009